(Article begins on next page)

Free and forced morphodynamics of river bifurcations

M. Redolfi*, G. Zolezzi*, M. Tubino*.

* Department of Civil, Environmental and Mechanical Engineering, University of Trento, Italy

Abstract

Water and sediment distribution by river bifurcations is often highly unbalanced. This may result from a variety of factors, like migration of bars, channel curvature, backwater effects, which promote an uneven partition of flow and sediment fluxes in the downstream branches, which we call "forcings". Bifurcations also display an intrinsic instability mechanism that leads to unbalanced configurations, as it occurs in the idealized case of a geometrically symmetric bifurcation, which we call "free", provided the width-to-depth ratio of the incoming flow is large enough. Most frequently, these free and forced mechanisms coexist, however their controlling roles on bifurcation dynamics has not been investigated so far. In this paper we address such question by proposing a unified free-forced modelling framework for bifurcation morphodynamics. Upstream channel curvature and different slopes of downstream branches (slope advantage) are specifically investigated as forcing effects typically occurring in bifurcations of alluvial channels. The modelling strategy is based on the widely used two-cell model of *Bolla Pittaluga et al.* (2003) here extended to account for the spatially non-uniform fluxes entering the bifurcation node. Results reveal that the relative role of free and forced mechanisms depends on the width to depth ratio falling above or below the resonant threshold that controls the stability of free bifurcations: when the main channel is relatively wide and shallow (super-resonant regime) the bifurcation invariably evolves towards unbalanced configurations, whatever the combination of curvature and slope advantage values, which instead control the bifurcation response under sub-resonant conditions. Detection of the resonant aspect ratio as a key threshold also releases the modelling approach from the need of parameter calibration that characterized previous approaches, and allows for interpreting under a unified framework the opposite behaviours shown by gravel bed and sand bed bifurcations for increasing Shields parameter values.

1 Introduction

Channel bifurcations control the downstream distribution of water and sediments in a variety of fluvial environments, such as deltas, alluvial fans, braided and anabranching rivers (*Slingerland and Smith*, 2004; *Kleinhans et al.*, 2013). Understanding their dynamics is therefore important for managing water resources and the flooding risk, predicting the long-term morphological evolution of channel networks and evaluating the effectiveness over time of river restoration projects aimed at reactivating a multi-thread configuration (e.g., *Habersack and Piégay*, 2007). Bifurcation dynamics also control instream processes in meander bends that mitigate the development of channel sinuosity through the occurrence of short cuts through point bars (*Grenfell et al.*, 2012; *van Dijk et al.*, 2014).

River bifurcations have been extensively studied through laboratory-scale physical models (*Federici and Paola*, 2003; *Bertoldi and Tubino*, 2007; *Bertoldi et al.*, 2009; *Le et al.*, 2018b), and mathematical models based on 1D (*Wang et al.*, 1995; *Bolla Pittaluga et al.*, 2003; *Kleinhans et al.*, 2013; *Salter et al.*, 2018), 2D (*Edmonds and Slingerland*, 2008; *Siviglia et al.*, 2013; *Le et al.*, 2018b,a) and 3D approaches (*Kleinhans et al.*, 2008). Along with field observations (e.g., *Zolezzi et al.*, 2006; *Kleinhans et al.*, 2012), these studies highlight the almost invariable tendency of bifurcations to produce an uneven distribution of flow and sediment transport, which results in a strong asymmetry of the channel width and bed elevation of downstream anabranches.

This type of unbalanced configuration is often promoted by various "forcing" effects that drive the bifurcation towards an unbalanced state, sometimes leading to the complete closure of one of the anabranches. Forcing factors include both upstream and downstream effects. Upstream effects comprise mechanisms that feed the bifurcating node with a topographically-driven uneven distribution of flow and transport rate, like the curvature of the upstream channel (*Kleinhans et al.*, 2008; *Hardy et al.*, 2011; *Sloff and Mosselman*, 2012) and the occurrence of migrating bars (*Bertoldi et al.*, 2009; *Bertoldi*, 2012) or steady bars (*Le et al.*, 2018b). Downstream effects include mechanisms that provide, locally or through backwater effects, a slope advantage to one of the distributaries (*Edmonds*, 2012; *van Dijk et al.*, 2014; *Zhang et al.*, 2017; *Salter et al.*, 2018). For purely illustrative purposes, Figure 1 shows real-world bifurcations with examples of these concepts. Figures 1a and 1b provide examples of bifurcations where one of these forcing factors is likely dominant: the upstream channel curvature (Figure 1a) and the slope advantage for the right bifurcate (Figure 1b). In Figures 1c and 1d these two forcings likely have comparable relevance. They might cooperate in the case of Figure 1c, because the chute channel detaches from the outer bank of the upstream channel bend, thus receiving most of the water and sediment input from upstream, and is also shorter than the other (left) bifurcate, thus having a slope advantage. On the contrary, they likely compete in the case of Figure 1d, because the shorter chute channel occurs on the inner bank of the upstream channel bend.

Interestingly, the unbalanced configuration can also result from an inherent instability mechanism, even in the absence of external forcings, as shown theoretically by *Wang et al.* (1995) and *Bolla Pittaluga et al.* (2003), and later demonstrated through laboratory and numerical studies (*Bertoldi and Tubino*, 2007; *Edmonds and Slingerland*, 2008; *Siviglia et al.*, 2013; *Salter et al.*, 2018). More recently *Redolfi et al.* (2016) provided an interpretation of such "free" bifurcations instability within the framework of the theory of morphodynamic influence of *Zolezzi and Seminara* (2001), showing that the unbalanced configuration arises when the bifurcation is able to exert an upstream morphodynamic influence that allows for the formation of an upstream steady bar. Such upstream morphodynamic influence theoretically occurs when the width to depth ratio exceeds a threshold "resonant" value, as originally defined by *Blondeaux and Seminara* (1985) in the theory of regular meanders. For small (sub-resonant) values of the width to depth ratio a symmetric free bifurcation keeps stable and equally distributes water and sediment fluxes in the downstream branches, while in the super-resonant regime such balanced configuration is no longer stable and the bifurcation invariably evolves towards an unbalanced configuration.

The above scenario suggests that in sub-resonant conditions the tendency towards unbalanced states observed in real rivers is mainly driven by external forcing factors, while in super-resonant conditions both free and forced mechanisms are likely interacting, though their respective roles have not been investigated so far. The question therefore arises to which extent the autogenic, free-instability mechanism or instead the external forcings affect the behaviour of natural bifurcations, and under which conditions those effects cooperate or compete to produce what is observed in such complex settings.

We aim at answering this question by taking the viewpoint of river bifurcations as dynamical systems for which a distinct role of the free and forced responses can be identified. This methodological distinction is based on the recognition that free and forced mechanisms display substantial differences in their evolutionary temporal and spatial scales. Similar approaches have proven to provide thorough insight in the study of other morphodynamic processes, like the dynamics of river bars in curved or meandering channels (*Seminara and Tubino*, 1989), where migrating free bars develop on a much faster scale than that required to shape the meander planform (*Tubino and Seminara*, 1990).

In this paper we cast within a unified theoretical framework previous results on free and forced bifurcations and consider two main forcing factors: the upstream effect exerted by an incoming curved channel and the downstream effect of slope advantage of one of the distributaries, which can derive from the different length of the distributaries, from differential downstream degradation/deposition (*Salter et al.*, 2018), or from backwater effects (e.g. *Edmonds*, 2012).

The analysis is based on the two-cell model originally proposed by *Bolla Pittaluga et al.* (2003), as extended by *Kleinhans et al.* (2008) to account for the curvature-driven secondary flow, and on the theoretical results of *Redolfi et al.* (2016). The analytical model prescribes physically-based, simplified nodal point relationships that enables us to explore the basic mechanisms that drive the water and sediment distribution at the node. As highlighted by *Wang et al.* (1995), the behaviour of the bifurcation depends on how the sediment is distributed with respect to the downstream transport capacity; sediment distribution is in turn determined by the transverse flow-exchange and gravitational effects on bed load transport just upstream the bifurcation node, as explained by *Bolla Pittaluga et al.* (2003).

2 Methods

Our model stems from the *Bolla Pittaluga et al.* (2003) two-cell approach, and is formulated to incorporate both free and forced bifurcation responses, and their interaction. It allows predicting how water and sediment fluxes delivered from the upstream main channel are drained by the

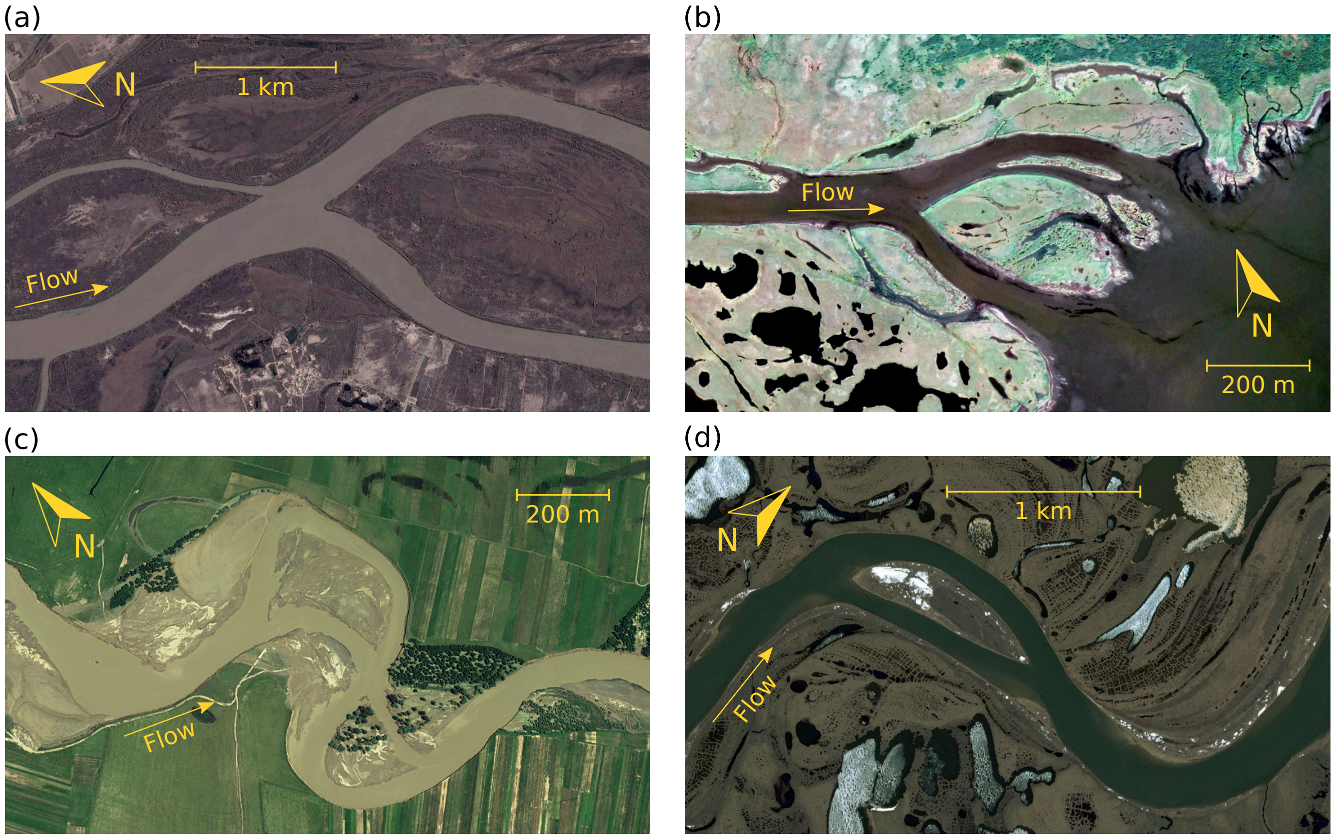

Figure 1: Satellite images showing illustrative examples of river bifurcations: (a) Tigris River near Baghdad (Iraq), $34°16' N$, $43°50' E$, with a curved upstream channel and downstream bifurcates having a nearly symmetrical channel geometry; (b) estuary in the Kamchatka Peninsula (Russia), $60°02' N$, $163°40' E$, where the left bifurcate likely covers a longer distance for the same elevation gap from the bifurcation node to the sea, suggesting a possible slope advantage for the left bifurcate; (c) bends with chute cutoffs in the meandering Siret River (Romania), $47°39' N$, $26°30' E$, with the cutoff channel initiating on the outer bank of an upstream channel bend and being shorter than the left bifurcate; (d) meandering River in the Ust-Chaun area (Russia), $68°42' N$, $170°35' E$, with the cutoff channel initiating on the inner bank of a bend and being shorter than the left bifurcate; from *Google Earth, Digital Globe (2018)*.

downstream anabranches, under different combination of external forcings.

The bifurcation geometry is sketched in Figure 2a, having an upstream, curved main channel of width W_a, slope S_a and radius of curvature R, which bifurcates in two downstream channels having width W_b and W_c and slope S_b and S_c, respectively. In the model, flow and sediment balances applied to two cells of length αW_a, which also accounts for transverse exchanges, rules the distribution of water (Q) and sediment (Qs) fluxes between the bifurcates, as represented in Figures 2b and 2c.

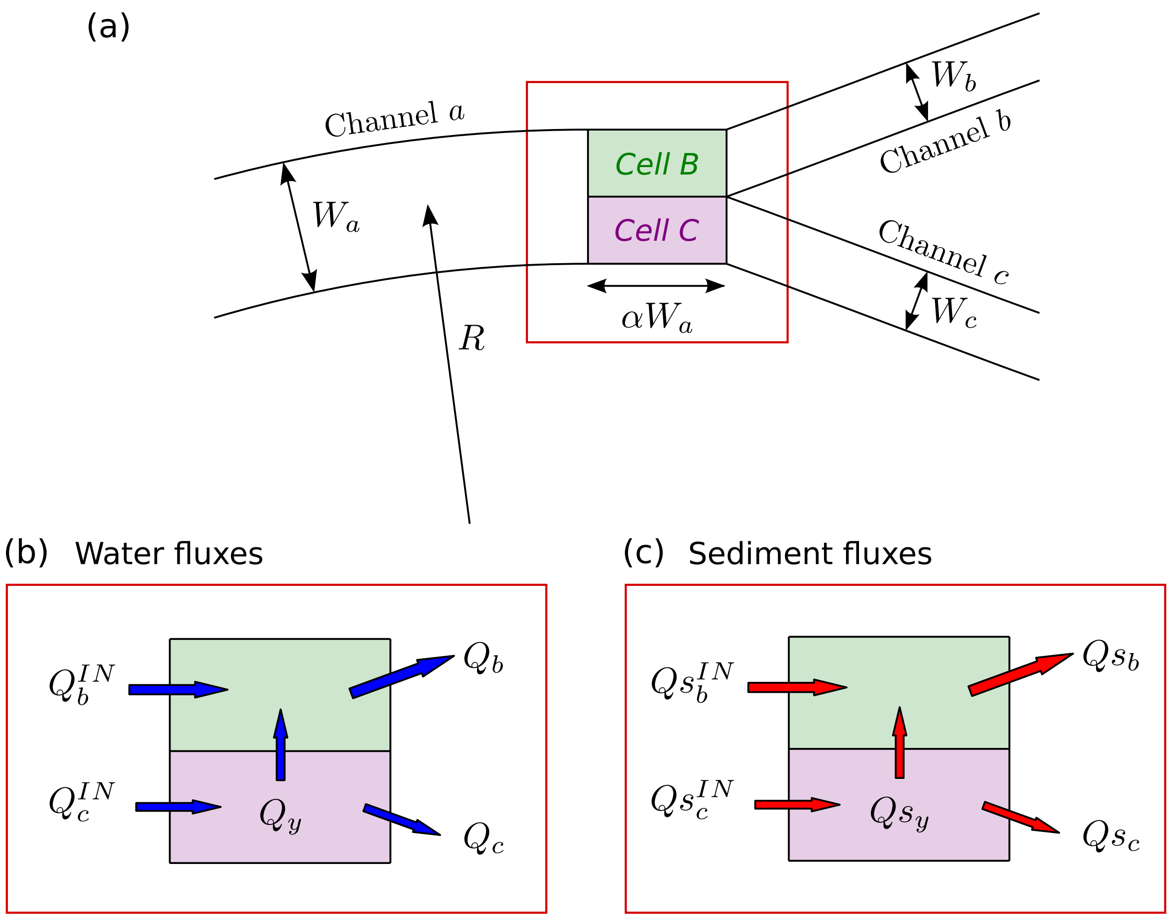

Figure 2: Bifurcation geometry and notation used in the mathematical model formulation: (a) planform view, showing the curved main channel, the two distributaries and the two cells; (b) and (c) water and sediment fluxes through the cells.

The model considers the effect of secondary flows associated with streamline curvature within the node cells (*Kleinhans et al.*, 2008), and includes an extension of such previous model to account for the non-uniform distribution for the entering water and sediment fluxes.

2.1 The free bifurcation

The core of the method is a model for a free bifurcation with perfectly symmetrical geometry and boundary conditions (i.e. with no curvature nor slope advantage) that follows the classic approach of *Bolla Pittaluga et al.* (2003). The flow and bed topography in the three channels result from a 1D mobile bed model, which can be solved once the following five matching conditions at the bifurcation node are specified: conservation of sediment and water fluxes (two conditions), energy conservation (i.e. water surface elevation) along each cell (two conditions), and a physically-based relation that prescribes how sediment fluxes are partitioned at the bifurcation node. This type of nodal point relation is the key to incorporate bifurcation morphodynamics within a simple 1D scheme, and accounts for the exchange of sediment between the two cells through the following relationship:

$$\underbrace{\frac{Qs_y/(\alpha W_a)}{Qs_a/W_a}}_{\text{sediment flux direction}} = \underbrace{\frac{Q_y/(\alpha W_a D_{abc})}{Q_a/(W_a D_a)}}_{\text{velocity direction}} - \underbrace{\frac{2r}{\sqrt{\theta_a}}\frac{\eta_b - \eta_c}{W_b + W_c}}_{\text{gravitational effect}}, \tag{1}$$

where the direction of the sediment flux is determined by the direction of velocity and by the gravitational effect induced by the transverse gradient of the bed elevation. The last term of Equation (1) is estimated according to the *Ikeda* (1982) formulation, where r is a dimensionless coefficient (e.g., *Baar et al.*, 2018), θ_a is the Shields stress in the main Channel a, η_b and η_c indicate the bottom elevation at the inlet of the distributary Channels b and c, respectively. The mean depth within the cell, defined as $D_{abc} = (2D_a + D_b + D_c)/4$, can be simplified to $D_{abc} = D_a$ as proposed by *Salter et al.* (2018).

The flow in the three anabranches is modelled using a classic 1D shallow water and Exner model, whose steady solution is simply an uniform flow. The water flow in each channel $i = \{a, b, c\}$ is given by:

$$Q_i = W_i\, c_i \sqrt{gS_i} D_i^{3/2}, \tag{2}$$

where g is the gravitational acceleration, D_i is the water depth and c_i is the dimensionless Chézy coefficient, which can be calculated as (*Engelund and Fredsoe*, 1982):

$$c_i = 6 + 2.5 \log \left(\frac{1}{2.5} \frac{D_i}{d_{50}} \right), \tag{3}$$

with d_{50} indicating the median grain size.

Similarly, the volumetric sediment flux is computed as:

$$Qs_i = W_i \sqrt{g \Delta d_{50}^3}\, \Phi \left(\theta_i, \frac{D_i}{d_{50}} \right), \qquad \theta_i = \frac{S_i D_i}{\Delta d_{50}}, \tag{4}$$

where Δ is the relative submerged density of the sediment, θ_i is the Shields stress and Φ is a function given by the sediment transport formula. Specifically, we used the *Parker* (1990) formula for gravel bed channels and the *Engelund and Hansen* (1967) formula for sand bed cases.

The free character of the bifurcation manifests itself in the symmetrical configuration of upstream and downstream channels, which determines water and sediment fluxes that enter and exit the cells (Figures 2b and 2c). First, the input fluxes Q_i^{IN} and Qs_i^{IN} that are delivered by the upstream channel into the node cells are uniform. Second, the absence of slope advantage (i.e. $S_b = S_c$) leads to the same water and sediment rating curves for the two bifurcates. Therefore, possible asymmetries of the output fluxes are not driven by the upstream/downstream conditions but can only derive from an uneven redistribution by the bifurcation node.

2.2 The forced bifurcation

Different forcing effects can be further incorporated in the free bifurcation model, to increase its ability of the model to represent real bifurcation configurations. The key to model those effects is to act on the upstream and boundary conditions imposed at the node cells, which practically implies considering non-uniform water and sediment fluxes entering the two node cells, and/or imposing different water and sediment rating curves for the two bifurcates. Such an approach has been already exploited by *Bertoldi et al.* (2009) when modelling how bifurcations dynamics can be affected by migrating bars, which were schematised as periodic temporal oscillations of water and sediment fluxes delivered to the node cells. Here we consider two different forcing effects: (i) a downstream slope advantage of one bifurcate with respect to the other one and (ii) the presence of a curved upstream channel.

A downstream slope advantage increases the probability for an unbalanced water and sediment flux towards the "advantaged" distributary. This effect can be taken into account by setting different values of S_b and S_c in Equations (2) and (4). This breaks the symmetry in the downstream rating curves, even if the other geometrical parameters remain equal between the two downstream branches. We quantify the slope advantage through the following parameter:

$$\Delta S = \frac{S_b - S_c}{S_b + S_c}, \tag{5}$$

with positive values of ΔS indicating that the outer bend bifurcate (Channel b of Figure 2a) is steeper than the inner bend bifurcate (Channel c).

We model the presence of an upstream bend (Channel a) feeding the bifurcation as does a channel with constant radius of curvature R. The curvature of the main channel leads to the formation of a spiral flow (Figure 3a), which in turn produces a shear stress in the transverse direction. Therefore, the bottom stress ends up being deflected by an angle ϕ_τ, which can be computed as (*Struiksma et al.*, 1985):

$$\tan(\phi_\tau) = -A\,\frac{D}{R}, \tag{6}$$

where D is the local water depth and A is the coefficient that defines the intensity of the secondary flow, given by:

$$A = \frac{2}{\kappa^2}\left(1 - \frac{1}{\kappa\, c}\right) \tag{7}$$

with $\kappa = 0.4$ indicating the Von Karman constant.

In the region where the flow is fully developed (i.e., far enough from the bend entrance), the flow characteristics do not vary along the channel, and the depth-averaged velocity is purely longitudinal. In these conditions, the deflection of the bed shear stress is compensated by a transverse gradient of the bed elevation (see Figure 3a) that is given by:

$$\frac{d\eta}{dy} = \frac{\sqrt{\theta}}{r}\,\tan\left(\phi_\tau\right), \tag{8}$$

(for mathematical details see Appendix A), which in turn generates non-uniform transverse profiles of water depth, longitudinal velocity and shear stress. Consequently, water and sediment fluxes feeding the two cells are not uniform but are mainly delivered towards the cell positioned at the outer bend (Cell B of Figure 3b).

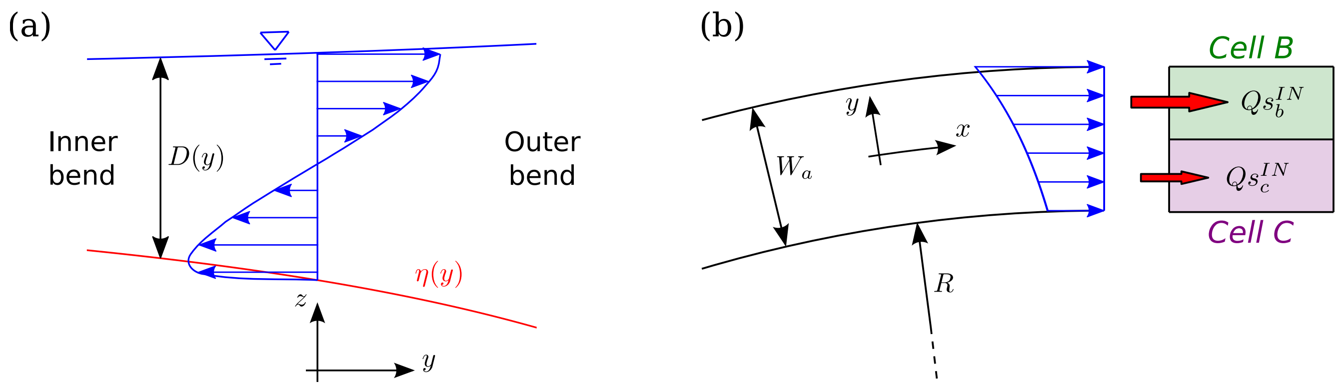

Figure 3: Illustration of the secondary flow solution in the upstream channel: (a) cross-sectional view, indicating the vertical profile of the transverse velocity (arrows), and the transverse profiles of bed elevation and water depth; (b) planimetric view, with the transverse velocity profile (arrows) and the associated sediment fluxes entering the cells (Qs_b^{IN} and Qs_c^{IN}).

Furthermore, as suggested by *Kleinhans et al.* (2008) the deviation of the bed shear stress given by Equation (6) is also active within the cells, so that the nodal point relation (1) needs to be extended as follows:

$$\underbrace{\frac{Qs_y}{\alpha Qs_a}}_{\text{sediment flux direction}} = \underbrace{\frac{Q_y}{\alpha Q_a}}_{\text{velocity direction}} - \underbrace{\frac{2r}{\sqrt{\theta_a}}\frac{\eta_b-\eta_c}{W_b+W_c}}_{\text{gravitational effect}} - \underbrace{A\frac{D_a}{R}}_{\text{spiral flow effect}}, \tag{9}$$

where D_a and θ_a are the average values of water depth and Shields stress in the upstream Channel a.

The above formulation is generally suitable for modelling bifurcations with arbitrary channel widths. However, for the purpose of analysing the interaction between the different mechanisms, also in comparison with previous works (e.g., *Bolla Pittaluga et al.*, 2015), we restrict our attention to the basic case where both the bifurcates have half the width of the main channel ($W_b = W_c = W_a/2$).

3 Results

The model solution can be expressed as a function of a few dimensionless parameters. First, the solution depends on the reference conditions, which are defined as the uniform flow and sediment transport in a straight channel with same slope, width and discharge of the main channel. Specifically, we need to prescribe three main parameters, namely the aspect ratio, the Shields stress and the relative roughness:

$$\beta_0 = \frac{1}{2}\frac{W_a}{D_0}, \qquad \theta_0 = \frac{S_a D_0}{\Delta d_{50}}, \qquad d_{s0} = \frac{d_{50}}{D_0}, \tag{10}$$

where zero subscript (e.g., D_0) indicates the reference conditions.

Second, the solution depends on the intensity of the forcing effects, which is specified through the normalized curvature W_a/R and the slope advantage ΔS.

In the following, we analyse the model outputs in terms of discharge asymmetry (*Bertoldi et al.*, 2009), which can be taken as a representative indicator of the bifurcation response:

$$\Delta Q = \frac{Q_b - Q_c}{Q_a}, \tag{11}$$

which may range from -1 (no flow in Channel b) to $+1$ (no flow in Channel c), with $\Delta Q = 0$ indicating balanced bifurcations.

3.1 The free bifurcation

The free bifurcation configuration is made by three straight channels without any slope advantage nor width or angle asymmetry, thus without external effects that may force an unbalanced configuration. In this condition the intuitive expectation would be a symmetrical bifurcation response, with an even distribution of downstream water and sediment fluxes. As illustrated in Figure 4, the balanced configuration ($\Delta Q = 0$) is indeed an equilibrium solution of the system. However, for relatively high values of the aspect ratio the balanced configuration becomes unstable, and one of the channels, indifferently, tends to dominate.

As highlighted by *Bolla Pittaluga et al.* (2003) this type of instability of the symmetric equilibrium solution does not necessarily lead to a complete closure of one branch, but new, unbalanced and stable equilibrium states are possible. In Figure 4, this is represented by the formation of a so called "pitchfork bifurcation" (e.g., *Wiggins*, 2003) in the equilibrium diagram, which occurs at β_0 near 13.5. The two unbalanced equilibrium configurations are physically sustained by the formation of an inlet step, i.e. a localized steep reach at the head of the largest flow-carrying bifurcate (*Bertoldi et al.*, 2009), which steers the sediment flux and thus satisfies the balance between sediment supply and transport capacity of the bifurcates.

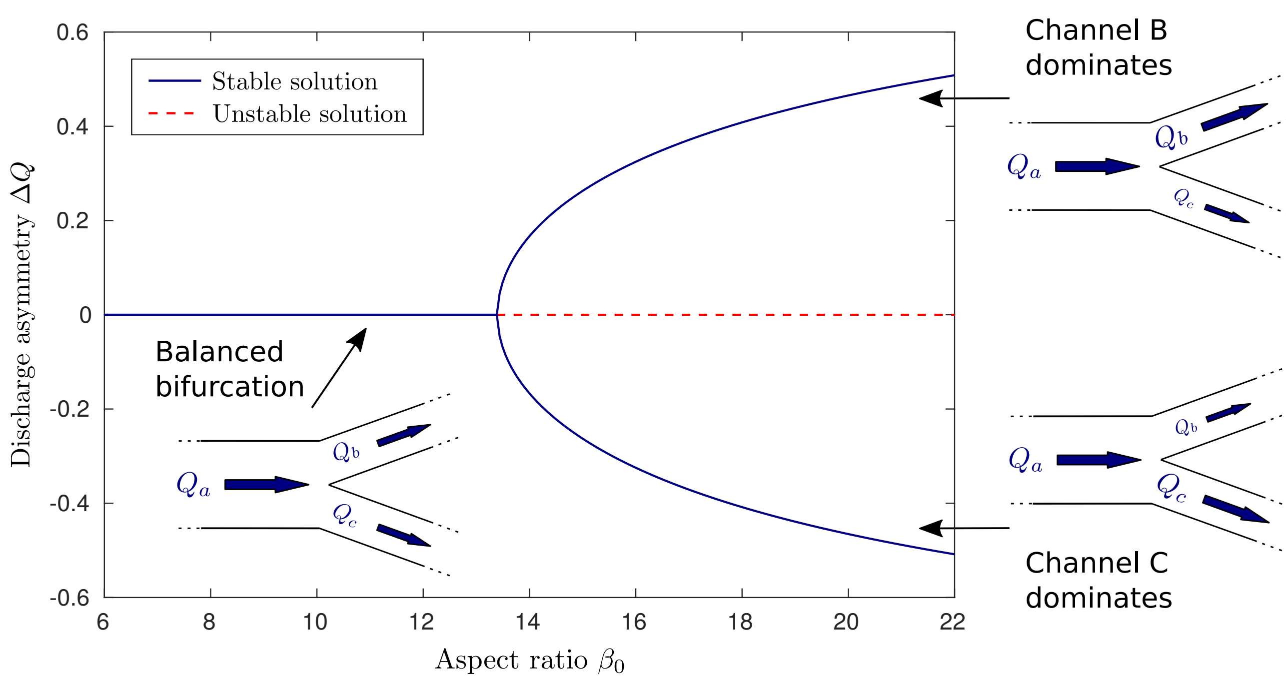

Figure 4: Equilibrium solutions of a free bifurcation (i.e. straight channel with no slope advantage) according to the two-cell model. Solid lines indicates stable solutions, while the dashed line represents an unstable equilibrium configuration. Parameters are $\theta_0 = 0.1$, $d_{s0} = 0.02$, $r = 0.5$; the *Parker* (1990) transport formula is used.

The critical point at which the pitchfork bifurcation appears is determined through a linear stability analysis (*Bolla Pittaluga et al.*, 2015), whose result can be expressed in the following general form:

$$\beta_C = \frac{r\alpha}{\sqrt{\theta_0}} \frac{4}{\Phi_D + \Phi_T - (3/2 + c_D)}, \tag{12}$$

whose coefficients are defined as:

$$c_D := \frac{D_0}{c_0}\frac{\partial c}{\partial D}\bigg|_{D_0}, \qquad \Phi_D := \frac{D_0}{\Phi_0}\frac{\partial \Phi}{\partial D}\bigg|_{D_0,\theta_0}, \qquad \Phi_T := \frac{\theta_0}{\Phi_0}\frac{\partial \Phi}{\partial \theta}\bigg|_{D_0,\theta_0}, \tag{13}$$

and represent the sensitivity of Chézy coefficient and of the dimensionless sediment transport rate to variations of water depth and Shields stress. The algebraic expressions of the coefficients c_D, Φ_D and Φ_T for the used formulae of *Parker* (1990) and of *Engelund and Hansen* (1967), as well as for the classical relation of *Meyer-Peter and Muller* (1948), are reported in Appendix B for the sake of clarity. Equation (12) represents a generalization of the formula proposed by *Bolla Pittaluga et al.* (2015) for arbitrary transport and friction formulae.

According to Equation (12), the critical aspect ratio is directly proportional to the cell length represented by α. In a 1D formulation, the parameter α needs to be empirically calibrated, resulting in rather different literature values, ranging from 1 (*Bolla Pittaluga et al.*, 2003) to 6 (*Bertoldi and Tubino*, 2007). This limitation has been solved by *Redolfi et al.* (2016), who developed an analytical linear solution of the fully 2D problem; in that formulation, the length of the upstream cells is resolved by the model itself, so that no specific calibration is needed.

The analysis of *Redolfi et al.* (2016) demonstrated that the emergence of an unbalanced solution in a free bifurcation depends on the formation of an upstream steady bar, which occurs when the bifurcation is able to exert a morphodynamic influence in the upstream direction (see Figure 5). As theoretically derived by *Zolezzi and Seminara* (2001) and experimentally observed by *Zolezzi et al.* (2005) any fixed geometrical disturbance can produce a permanent upstream bed deformation, usually taking the form of a steady bar, when the channel is wide and shallow enough for the aspect ratio of the main channel to exceed the resonant threshold, β_R, as originally defined in the theory of regular meanders by *Blondeaux and Seminara* (1985). Therefore, under super-resonant conditions ($\beta_0 > \beta_R$) the bifurcation node - as a fixed geometrical disturbance - can trigger such an upstream morphodynamic influence. This is essentially the physical mechanism behind the mathematical instability of the balanced equilibrium solution, which therefore makes a free bifurcation unbalanced.

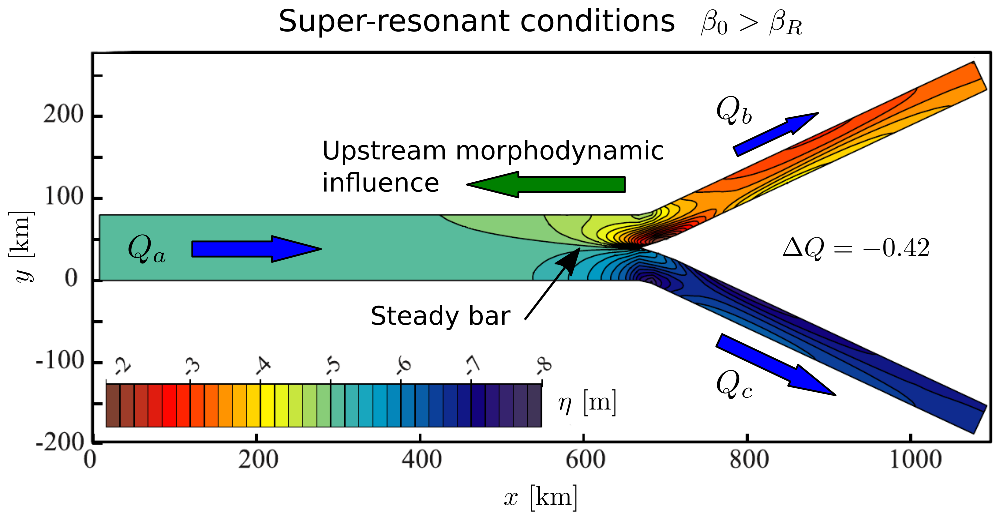

Figure 5: Map of bed elevation and water distribution in a free bifurcation from the numerical simulations of *Edmonds and Slingerland* (2008), adapted from their Figure 5b. The equilibrium configuration is made unbalanced by the formation of an upstream steady bar, which deviates most water and sediment fluxes towards the right bifurcate. According to *Redolfi et al.* (2016) this is an effect of the upstream morphodynamic influence exerted by the bifurcation node, which occurs when the aspect ratio of the upstream channel β_0 exceeds the resonant threshold β_R.

The computation of the resonant aspect ratio requires the solution of a fourth-order polynomial, which can be readily obtained using the available Matlab code (see Acknowledgements Section). The resulting values for gravel bed and sand bed river channels as a function of the relevant dimensionless parameters are reported in Figures 6a and 6b, respectively. For sand bed rivers the Chézy coefficient is independently fixed, rather than derived from Equation (3), to account for the higher drag exerted by bedforms, also consistently with previous applications (*Edmonds and Slingerland*, 2008). In gravel bed channels β_R increases with both the Chézy coefficient and the Shields stress, which explains the tendency of bifurcations to stabilize when increasing θ_0 (*Bolla Pittaluga et al.*, 2015). Conversely, in sand bed channels the resonant threshold tends to decrease with the Shields stress, which explains the opposite effect of θ_0 observed by *Edmonds and Slingerland* (2008). Consistently with *Bolla Pittaluga et al.* (2015) the different behaviour of sand bed and gravel bed channels is related to the different response of the dimensionless sediment transport rate to variations of the Shields stress (which depends on the transport formula) rather

Table 1: List of datasets used to evaluate the resonance criterion for bifurcation instability.

Dataset	Method	Bed material	# of cases	β_0	θ_0
Bertoldi and Tubino (2007)	Laboratory	gravel	25	4.9 – 26.3	0.042 – 0.099
Edmonds and Slingerland (2008)	Numerical	sand	11	8	0.80 – 2.19
Siviglia et al. (2013)	Numerical	gravel	18	3.5 – 24.0	0.060 – 0.200
Zolezzi et al. (2006)	Field	gravel	6	9.5 – 14.5	0.053 – 0.088
Bolla Pittaluga et al. (2015)	Field	sand	11	16.9 – 77.1	0.30 – 1.16

than an effect of a gradient in the water surface elevation near the bifurcation, as suggested by *Edmonds and Slingerland* (2008).

Alternatively, the resonant aspect ratio can be calculated though the approximate expression by *Camporeale et al.* (2007):

$$\beta_R = \frac{\pi}{2\sqrt{2}} \frac{c_0\sqrt{r}}{\theta_0^{1/4}} \frac{1}{\sqrt{\Phi_D + \Phi_T - (3/2 + c_D)}}, \tag{14}$$

which provides rather accurate estimates of β_R for sand bed channels, while it gives slightly underestimated values for gravel bed cases (up to -13% for the range of parameters in Figure 6a).

The resonant threshold provides a simple criterion to determine if a free bifurcation remains balanced or tends to evolve towards unbalanced states. To test this criterion we used the literature datasets listed in Table 1, which include gravel and sand bifurcations measured in the field, modelled numerically and reproduced in laboratory-scale physical models. For each of the 71 bifurcations the different authors provided observation of their balanced/unbalanced state and the basic flow parameters, which were used to compute the resonant threshold and the parameter $(\beta_0 - \beta_R)/\beta_R$ representing the relative distance to resonance. We set $r = 0.5$ for all cases except for the *Edmonds and Slingerland* (2008) experiments, for which an equivalent $r \simeq 0.35$ value was needed to match the default $\alpha_{bn} = 1.5$ value of their Delft3D formulation (e.g., *Lesser et al.*, 2004). Results reported in Figures 6c and 6d show that balanced bifurcations (closed markers) tend to stay below the dashed line (i.e. sub-resonant conditions), while all the unbalanced bifurcations (open markers) are located above the dashed line (i.e. super-resonant conditions), independently of the Shields stress. It is worth noting that the resonant criterion also captures the numerical results of *Edmonds and Slingerland* (2008), who demonstrated that balanced solutions in sand bed channels tends to become unstable with increasing θ_0. The above analysis confirms that the reso-

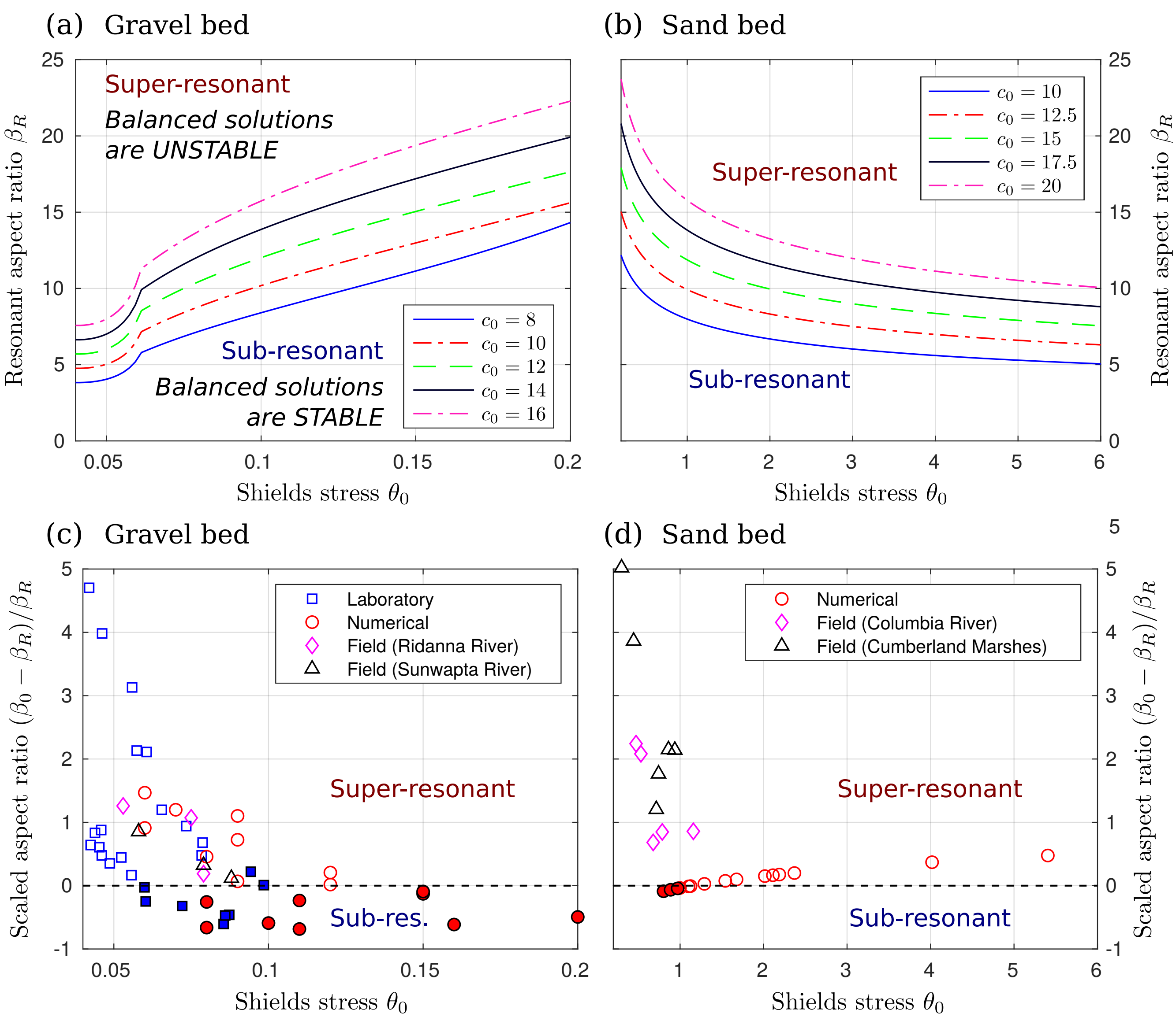

Figure 6: (a) and (b) Resonant aspect ratio β_R for gravel and sand bed channels as a function of Shields stress and Chézy coefficient. Under sub-resonant conditions (i.e. $\beta_0 < \beta_R$) the balanced bifurcation configuration is stable, while in super-resonant channels ($\beta_0 > \beta_R$) the instability mechanism makes the bifurcation unbalanced. (c) and (d) Observations of the balanced (close markers) or unbalanced (open makers) state of the bifurcation as a function of Shields stress and relative distance from the resonant threshold (scaled aspect ratio), for each of the 71 bifurcations listed in Table 1.

nant threshold correctly predicts stability of both gravel and sand bed bifurcations, with the key advantage of avoiding the need of calibrating a specific parameter like the α required by previous theoretical models (e.g., *Bolla Pittaluga et al.*, 2003, 2015).

The value of α that makes the nonlinear two-cell model consistent with the 2D theory can be determined by simply setting $\beta_C = \beta_R$ in Equation (12). Results reported in Figure 7 show a significant dependence of α on the reference conditions (θ_0 and c_0), which explains the large variability emerging in the literature. We notice that this estimate is strictly valid in the neighbour of the instability threshold, while for larger β it provides an upper limit of the optimal value for predicting the discharge asymmetry, as suggested by both laboratory observations and theoretical considerations (*Bertoldi and Tubino*, 2007; *Redolfi et al.*, 2016).

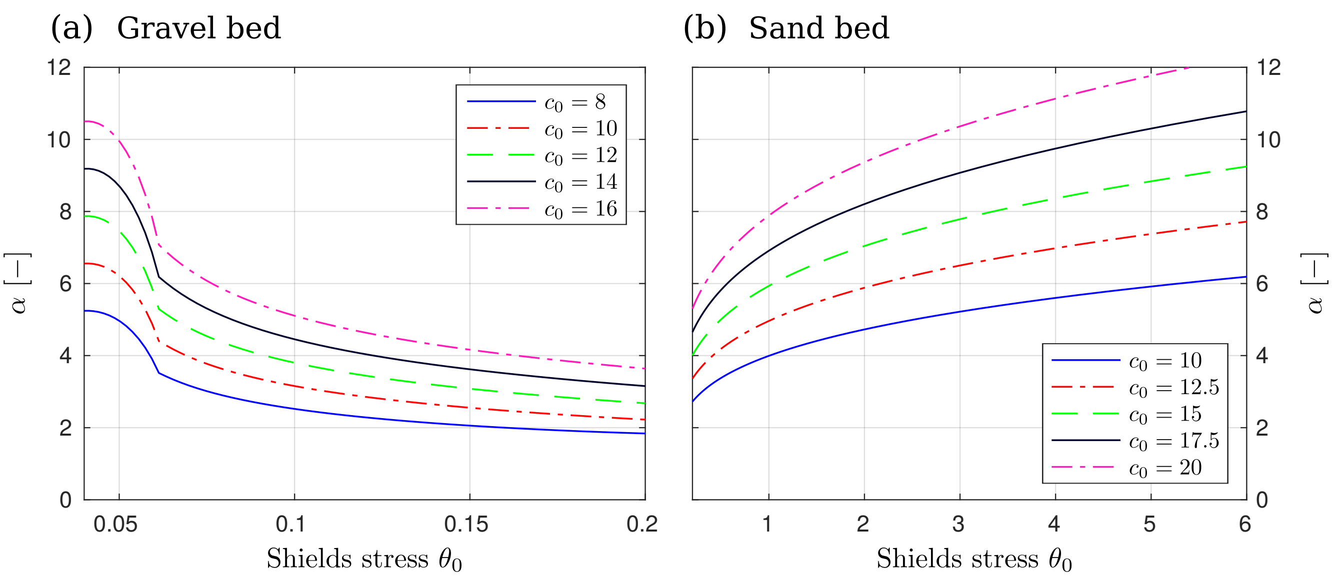

Figure 7: Values of the parameter α that make the two-cell model consistent with the linear 2D theory of *Redolfi et al.* (2016): (a) gravel bed channels, (b) sand bed channels.

Data of Table 1 include field measurements of natural bifurcations, which are not necessarily free. In this case the observed asymmetry may be not fully ascribed to the free instability mechanism but it may also be enhanced by the presence of the external forcings. The analysis of forcing effects and their interaction with the free instability mechanism is the main subject of the next section.

3.2 The forced bifurcation

Natural bifurcations are rarely free because of a number of forcing effects, including curvature of the main channel, different bifurcation angles, slope advantages, migration of bars, presence of obstacles, differential downstream sedimentation (e.g. *Van der Mark and Mosselman*, 2013; *van Dijk et al.*, 2014; *Le et al.*, 2018b,a; *Salter et al.*, 2018).

In the presence of a forcing effect, for example a curvature of the main channel, the equilibrium diagram of Figure 4 changes its topology. Specifically, as illustrated in Figure 8a, the equilibrium solution at relatively low values of β_0 is not balanced (i.e. $\Delta Q = 0$) and as expected more water is flowing towards the outer bend. When β_0 increases, the effect of the channel curvature tends to be amplified by the bifurcation, resulting in a more and more unbalanced configuration. However, at a given β value two additional equilibrium solutions form (a so called "imperfect pitchfork bifurcation", see for example *Golubitsky and Schaeffer*, 1979). One of them is unstable (dashed line in Figure 8a), while the more unbalanced solution is stable. This suggests the possibility for the bifurcation to attain a different, stable equilibrium point, where most of water and sediment fluxes are deviated towards the inner bend bifurcate.

The behaviour of the equilibrium solutions for different values of the dimensionless channel curvature W_a/R is illustrated in Figure 8b. When $W_a/R = 0$ (straight channel) we obtain again the solution of Figure 4, here represented in terms of the distance from the resonant point, so that the pitchfork "bifurcation" appears at $(\beta_0 - \beta_R)/\beta_R = 0$. By analysing the effect of increasing curvature two relevant aspects emerge. First, the increase of the discharge asymmetry with channel curvature is significantly more pronounced at relatively small values of the channel aspect ratio (i.e. in the sub-resonant regime), where lines corresponding to different curvature values are more spaced apart, while at higher (i.e., super-resonant) aspect ratios the effect of curvature is minimal. Second, the value of the aspect ratio at which the second stable solution forms increases with channel curvature. For example, when $W_a/R = 0.1$ an aspect ratio 50% higher than the resonant value is needed to allow for the existence of multiple stable solutions.

The possibility of obtaining multistable solutions depending on channel curvature and aspect ratio is better illustrated in Figure 9a. While under sub-resonant conditions the equilibrium

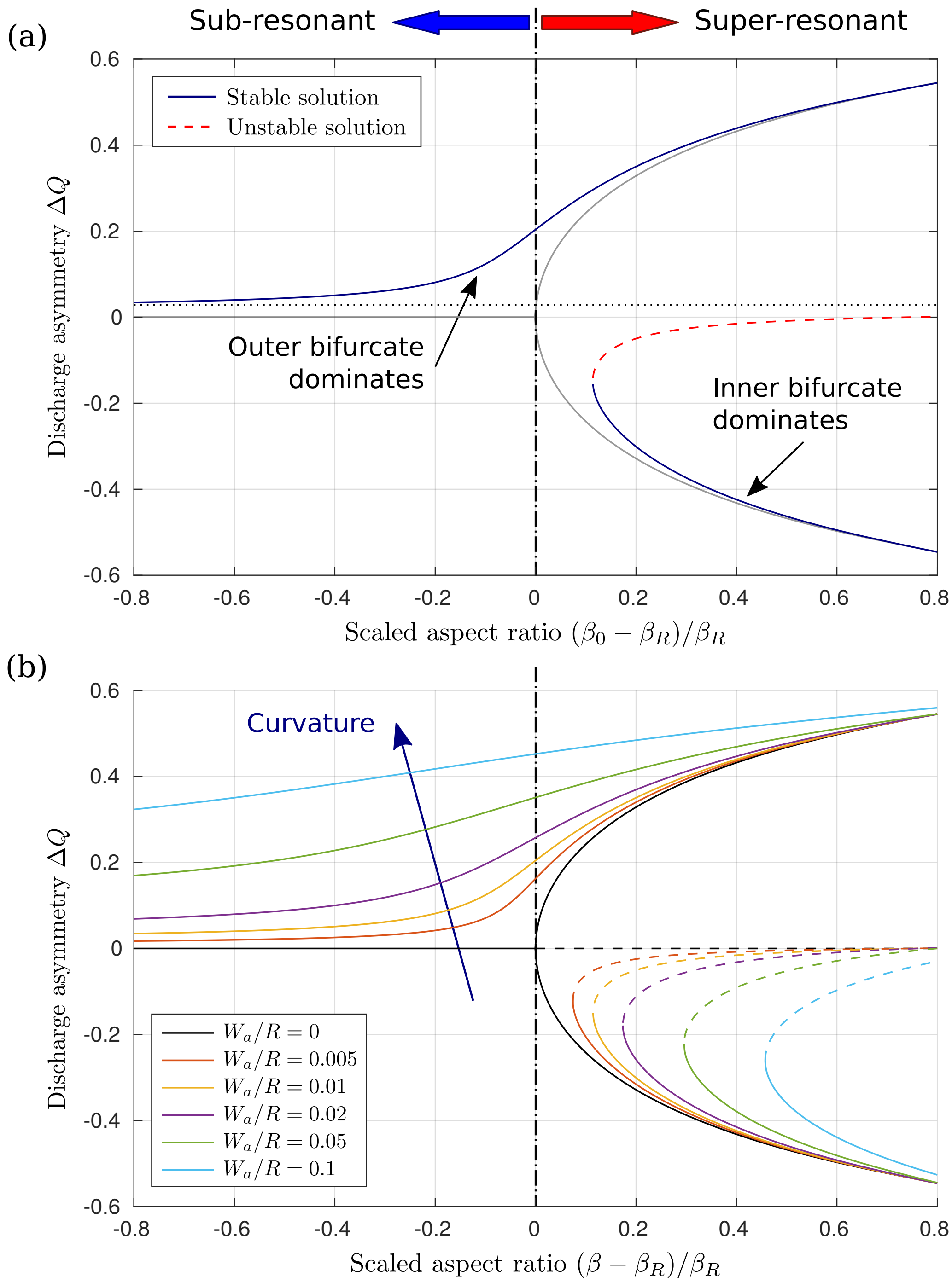

Figure 8: Stable (solid lines) and unstable (dashed lines) equilibrium solutions for a bifurcation with a curved upstream channel, as a function of the scaled aspect ratio. (a) Example with fixed curvature ($W_a/R = 0.01$), where the dotted line indicates the discharge ratio at the cell entrance and the grey lines represent the reference, “free” solution. (b) Effect of increasing curvature values. The vertical dashed line separates the sub-resonant (left) from the super-resonant (right) region.

solution is unique, two stable equilibrium solutions exist in super-resonant conditions. However, if the curvature is sufficiently large (depending on $(\beta_0 - \beta_R)/\beta_R$) only the solution for which the outer channel dominates is possible.

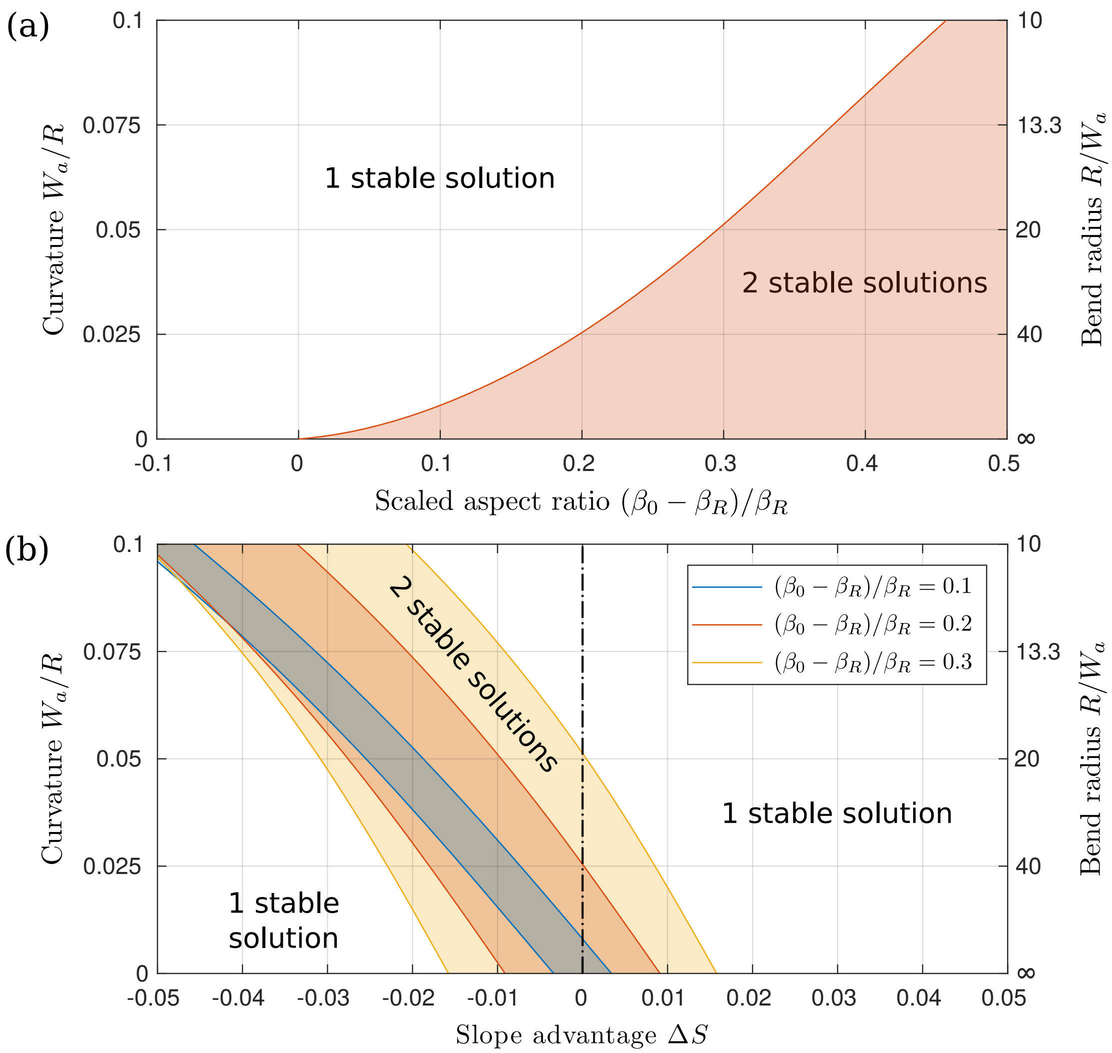

Figure 9: Stability diagram indicating regions where two stable equilibrium solutions exist depending on: (a) scaled aspect ratio and channel curvature (no slope advantage); (b) the combined effect of channel curvature and slope advantage, for different values of the scaled aspect ratio.

The above depicted scenario is characteristic of imperfect systems, and turns out to be similar when analysing different kind of forcings. Here we do not specifically report on the effect of the slope advantage but we directly focus on the more interesting analysis of its interaction with the curvature of the upstream channel.

In some cases the effect of main channel curvature can be compensated by a slope advantage that tends to steer water and sediment flows towards the steeper inner bend bifurcate (e.g., *Klein-*

hans et al., 2008; *van Dijk et al.*, 2014). Analysis of the combined effect of the different forcings on the discharge asymmetry gives the results illustrated in Figure 10a, which confirms that for a sub-resonant bifurcation a channel curvature can be compensated by a gradient advantage. When $\Delta S = -0.01$ the discharge asymmetry is the same as the upstream asymmetry independently of β_0, while for higher slope advantages the bifurcation tends to distribute water towards the inner bend channel, in a greater proportion when β_0 increases. However, the scenario dramatically changes when the aspect ratio exceeds the resonant threshold (i.e. super-resonant conditions). In this case, equilibrium solutions are never balanced, with one of the two bifurcates becoming dominant for any combination of curvature and slope advantage. In Figure 10b one sees that under sub-resonant conditions the equilibrium ΔQ varies smoothly with the slope advantages, while when β_0 exceeds β_R sharp transitions and hysteresis are expected when varying ΔS.

In general the discharge asymmetry depends on slope advantage and curvature as illustrated in Figure 11. Under sub-resonant conditions (Figure 11a) variations of ΔQ are always smooth, and the effect of channel curvature can be always compensated by negative values of ΔS. Conversely, under super-resonant conditions (Figure 11b) the bifurcation is never balanced, and there is a well-defined region (black oblique stripes) in the forcing parameters space where two stable solutions coexist. The width of such bi-stable region depends on the distance from the resonant point as depicted in Figure 9b.

It is important to remark that all our diagrams have been obtained by considering fixed values of relative roughness ($d_{s0} = 0.02$), Shields stress ($\theta_0 = 0.1$) and *Ikeda* (1982) coefficient ($r = 0.5$), and the same transport (*Parker*, 1990) and friction (Equation (3)) formulae. Nevertheless, from a qualitative point of view, model results, and therefore their interpretation, are fully independent of the specific choice of flow parameters values and closure relations for sediment transport.

4 Discussion

The present work has built on previous analyses to propose a theoretical framework for river bifurcations within the context of 1D morphodynamic modelling that accounts for key 2D ingredients at the entrance of the bifurcation node and in the fluxes delivered by the upstream channel.

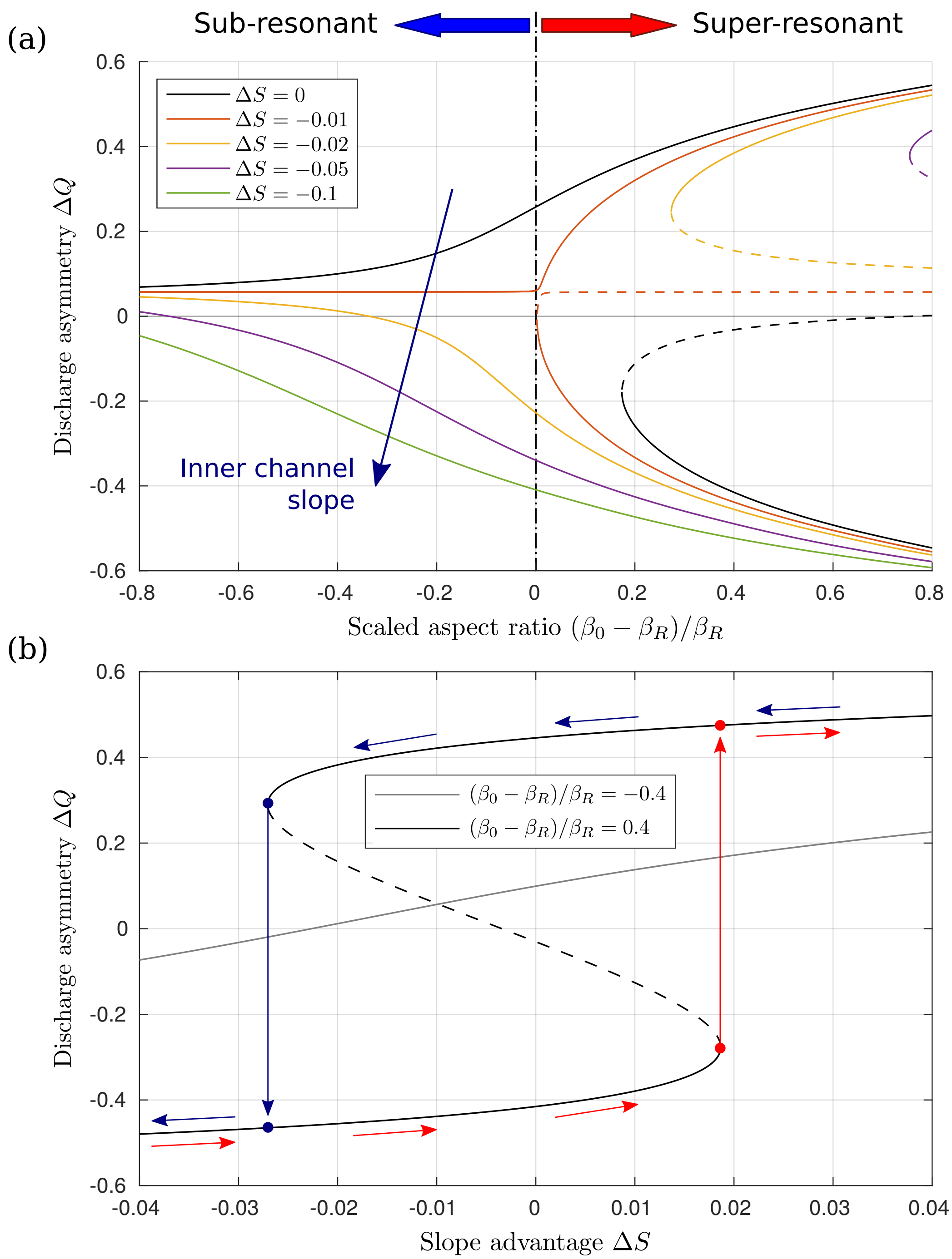

Figure 10: Effect of the slope advantage on a curved ($W_a/R = 0.02$) bifurcation. (a) Equilibrium solutions as a function of the aspect ratio β_0. (b) Equilibrium solutions as a function of the slope advantage under sub-resonant (grey line) and super-resonant (black lines) conditions. Solid and dashed lines indicate stable and unstable solutions respectively, while arrows indicate possible trajectories when increasing (red arrows) or decreasing (blue arrows) ΔS.

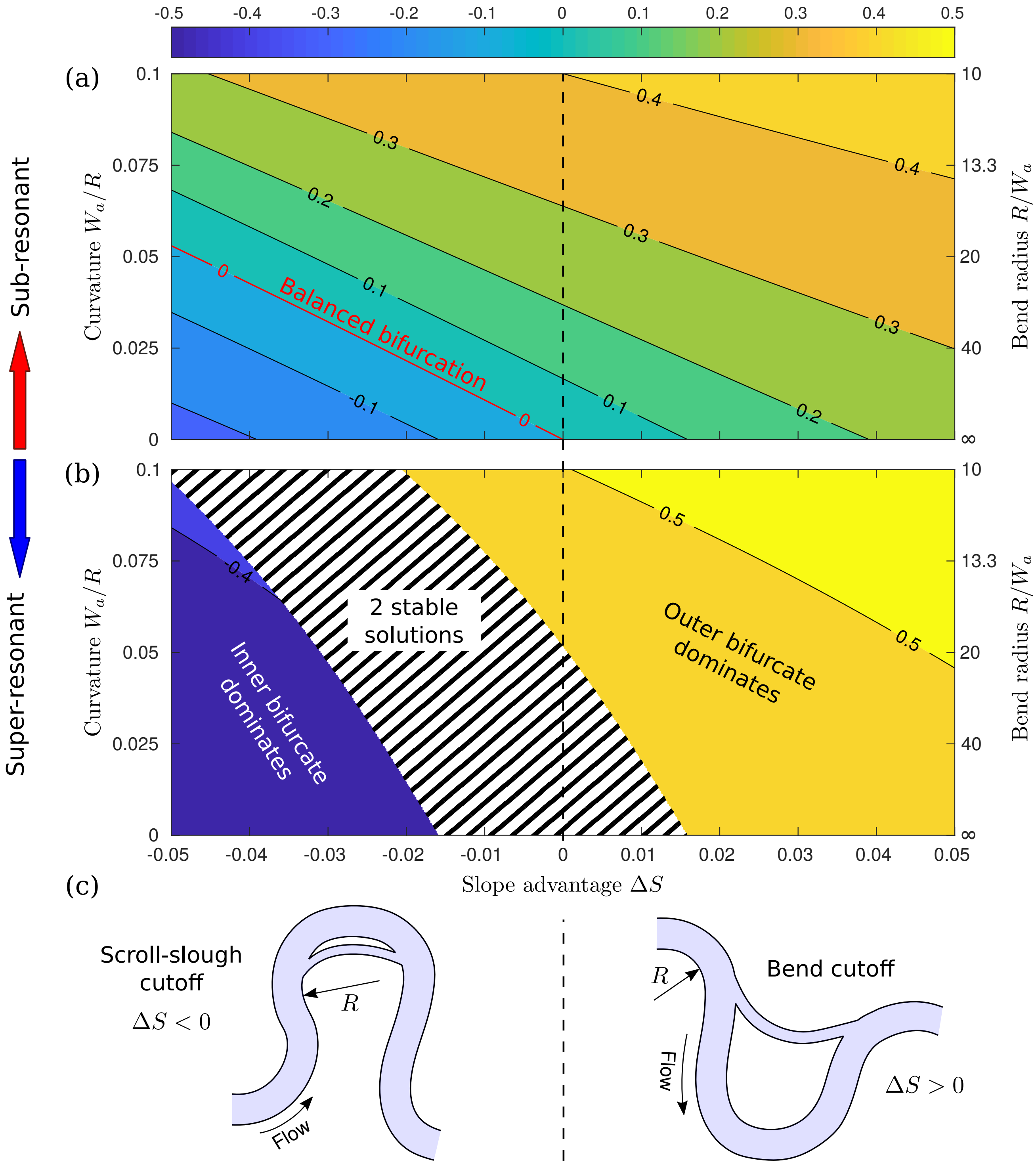

Figure 11: Discharge asymmetry as a function of curvature and slope asymmetry: (a) sub-resonant conditions ($(\beta_0 - \beta_R)/\beta_R = -0.3$); (b) super-resonant conditions ($(\beta_0 - \beta_R)/\beta_R = 0.3$), with black oblique stripes indicating the region where two stable solutions exists. (c) example of different slope advantages in meanders chute cutoff. Left: steeper inner channel ($\Delta S < 0$); right: steeper outer channel ($\Delta S > 0$).

Here we discuss (i) the main implications of our findings and the potential of the proposed approach for the interpretation of bifurcation dynamics, as it emerges from both observations and modelling; (ii) the significance of the equilibrium analysis for time-dependent processes; (iii) the need to clarify the specific use of the wording "instability" when addressing bifurcation dynamics, in the light of our findings and in the context of previous studies; (iv) applicability and limitations of our approach.

Enhanced insight on bifurcation morphodynamics

The core of the model lies in incorporating in the 1D scheme of *Bolla Pittaluga et al.* (2003) (i) the resonant aspect ratio as threshold for bifurcation stability (*Redolfi et al.*, 2016) and (ii) the effect of the forcing factors, through a proper modelling of the water and sediment fluxes delivered from the upstream channel and accepted by the downstream bifurcates. These fluxes are laterally symmetrical in the case of a purely free bifurcation, while the opposite occurs when adding forcing effects, which are almost invariably observed in real settings. Among the broad variety of forcing factors that characterize natural river bifurcations, here we addressed the isolated and the combined effect of an upstream channel curvature and a gradient advantage between the downstream branches.

A first important insight allowed by the proposed approach is the confirmation of the key role of the resonant aspect ratio on bifurcation behaviour, and an in-depth quantitative understanding of how the bifurcation response depends on the relative distance of the channel-forming aspect ratio value from such resonant threshold. This is supported with an analysis of an unprecedented number of laboratory, numerical and field data, for both gravel-bed and sand bed streams. The stability criterion based on the resonant threshold explains the loss of stability with increasing Shields stress of balanced sand bed bifurcations observed by *Edmonds and Slingerland* (2008), which is simply the consequence of adopting different transport and friction formulae. Compared with previous stability criteria, the analysis based on resonance offers the key advantage that it does not require the calibration of a specific parameter like the k exponent of *Wang et al.* (1995) or the α length parameter of *Bolla Pittaluga et al.* (2003, 2015).

Interestingly, the role of the free instability mechanism is not limited to ideal, geometrically symmetric bifurcations with symmetrical boundary conditions, but it is also a key controlling factor for complex, forced bifurcations. Consequently, also the response of bifurcation to the external forcings highly depends on channel conditions with respect to resonance. Under sub-resonant conditions, the bifurcation behaviour is relatively simple, as it is perfectly balanced for free, symmetrical bifurcations and mostly dominated by the forcing effects when they are present. On the contrary, under super resonant conditions balanced equilibrium configurations are never stable, so that the bifurcation always tends to highly asymmetric equilibrium states. Here, multiple stable solutions are possible, including counter-intuitive configurations where the inner bifurcate prevails, which suggests the possibility of complete shifts and hysteresis in the bifurcation response to changing conditions (*Scheffer et al.*, 2001).

The whole picture yields a clear, physically-based key to interpreting results of field observations and numerical models, which at times displayed behaviours that could not be given a fully exhaustive explanation. An example is provided by the result of *Kleinhans et al.* (2008), based on a three-dimensional model of a curved bifurcation with different channel gradients. These results revealed a "dramatic effect" of the width to depth ratio on discharge distribution and overall bed morphology, with the bifurcation switching from a dominant inner-bend bifurcate to a dominant outer-bend bifurcate, which indicates that the bifurcation behaviour "bifurcates" at a certain width between $W_a = 288\,\mathrm{m}$ and $378\,\mathrm{m}$ (see Section 4.5 of *Kleinhans et al.*, 2008). By applying our proposed modelling framework, and using the same closure relation and flow conditions as in the numerical experiments, it turns out that the observed range of widths correspond to the transition from from sub-resonant (Figure 12a) to super-resonant (Figures 12b and 12c) conditions. This transition can explain the fairly different morphological evolution upstream the bifurcation: under sub-resonant conditions the bifurcation does not significantly affect the upstream bed elevation (dashed line of Figure 12a), while under super-resonant conditions the upstream morphodynamic influence triggered by the bifurcation induces the formation of steady bars in the upstream channel (Figures 12b and 12c), which affect how discharge is downstream distributed.

Super-resonant conditions are not rare in nature, insofar as gravel bed rivers tends to behave

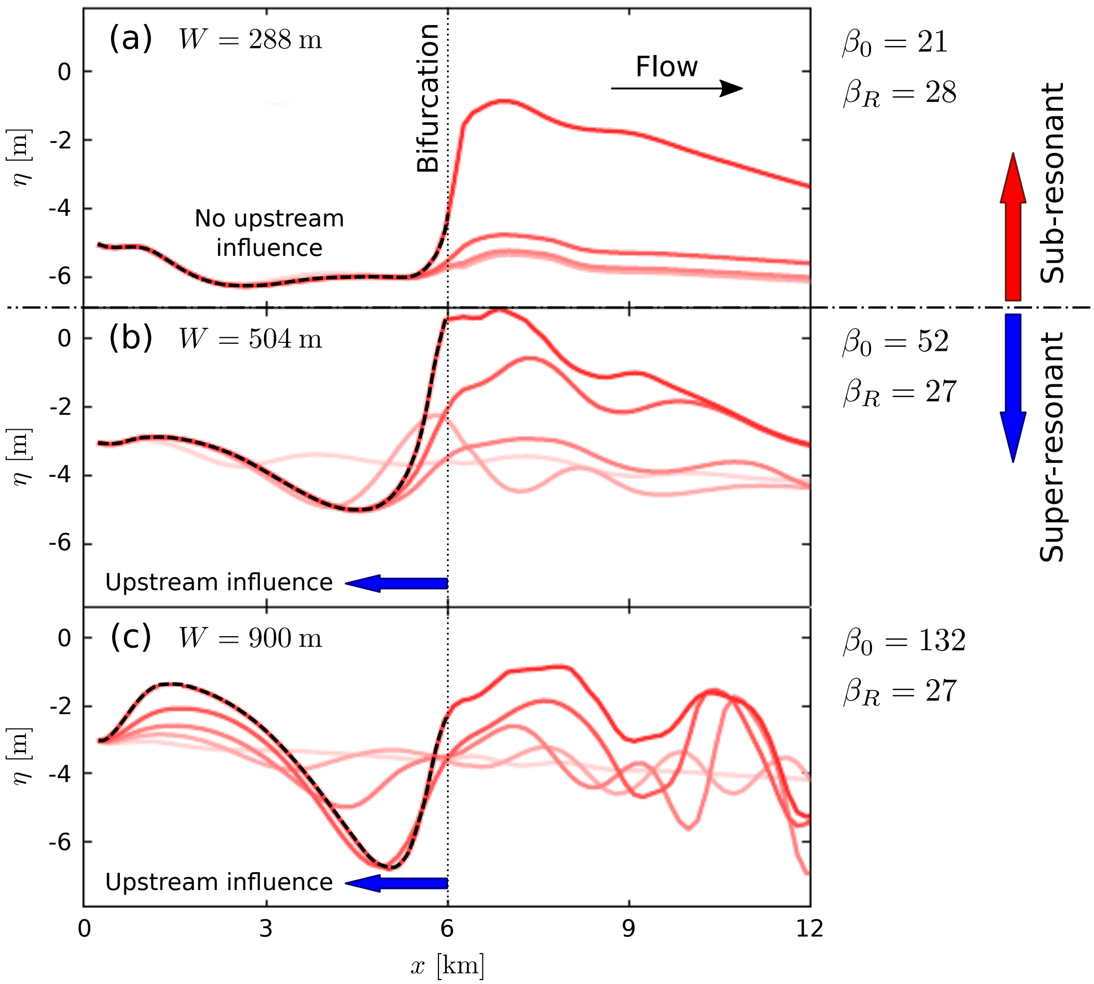

Figure 12: Profiles of bed elevation at the outer bank of a curved channel that bifurcates at $x = 6\,\mathrm{km}$, according to the numerical simulations of *Kleinhans et al.* (2008), adapted from their Figure 12 (long bend series). (a) Sub-resonant conditions; (b) and (c) super-resonant conditions. Lines from light to dark indicate advancing time. The dashed line indicates the final bed profile upstream the bifurcation, which shows significant oscillations only when the upstream channel falls under super-resonant conditions.

super-resonantly, especially for near-threshold (i.e. low Shields stress) channels (*Zolezzi et al.*, 2009). This confirms the tendency of balanced bifurcations to become unstable when the fixed bank hypothesis is released so that channels are free to reach their regime width (*Miori et al.*, 2006).

When different forcing effects are simultaneously acting they can compensate themselves (e.g *Kleinhans et al.*, 2008; *van Dijk et al.*, 2014; *Kleinhans et al.*, 2013), leading to a nearly balanced configuration. For example a gradient advantage in a scroll-slough chute cutoff of a meander bend (Figure 11c) can balance the opposite effect of the channel curvature. However, this is possible only if the upstream channel is in sub-resonant conditions, so that the bifurcation is intrinsically stable. On the contrary, under super-resonant conditions the bifurcations tends to propagate its morphodynamic influence in the upstream direction, so that the discharge partition is always highly unbalanced, independently of the upstream and downstream conditions.

Similar results can be found when other kind of forcing effects are interacting with the free instability mechanism, as emerging in the analysis of *Bertoldi et al.* (2009) about the effect of downstream-migrating alternate bars on the bifurcation dynamics. In that context, different characteristic regimes have been identified depending on the channel aspect ratio with respect to a critical threshold. For relatively small β_0 the bifurcation is essentially balanced with discharge oscillations around $\Delta Q = 0$ caused by the passage of bars, while for higher β_0 unbalanced states are observed. In this latter case the bifurcation can be either "bar perturbed" (small oscillations around a stable unbalanced state) or "bar dominated" (frequent switching of the bifurcation between opposite, highly unbalanced states). A diagram similar to Figure 10b can be used to interpret the different scenarios: essentially balanced solutions occur under sub-resonant conditions, while super resonant conditions yield highly unbalanced solutions, which are "bar perturbed" when the variations of the forcing factor are relatively weak, or "bar dominated" when forcing effect is strong enough to make the solution jumping between opposite states.

Quasi-equilibrium and temporal scales: the present work in a broader context

Our analysis is focused on steady equilibrium configurations, where both upstream and downstream channels are considered in planimetric and altimetric equilibrium. Strictly speaking, this is rarely the case of natural bifurcation, because forcing effects are usually varying in time. Nevertheless, as long as their rate of change is slow as compared with the intrinsic time scale of the bifurcation, the response of the system can be studied as a sequence of quasi-equilibrium states. This allows us to interpret the action of downstream migrating bars, as well as the analogous effect of the migration of the upstream meander (*Kleinhans et al.*, 2011), by means of equilibrium diagrams like those of Figure 10.

Similarly, the quasi-steady analysis can be applied for interpreting the effect of downstream variations, provided they are comparatively slow. For example, in the depositional systems investigated by *Salter et al.* (2018), the interaction between the bifurcation and the downstream bifurcates leads to autogenic temporal oscillations of channel slope and discharge asymmetry. This process evolves on a time scale that is proportional to the length of the downstream bifurcates, which is usually much longer than the intrinsic time scale of the bifurcation evolution (see *Miori et al.*, 2006). Therefore, focusing on the local behaviour of the bifurcation node, such downstream mechanisms can be considered as an external forcing effect, coherently with the definition adopted in the present work.

This provides a worthwhile example of how the definition of the forcing factors depends in general on the spatial and temporal scales under consideration. An analogous concept is at the core of classical theoretical studies on bar-bend interactions in river meanders (e.g., *Tubino and Seminara*, 1990), which pointed out how the dynamics of sediment bars inside meandering channels depends on the interaction between the free instability mechanisms that causes spontaneous development of migrating bars, and the effect of the variable meander curvature. In general also the channel curvature is not fixed but changes in time as the meander develops. However, as long as the two mechanisms act at different time scales, the planform evolution being a much slower process, when focusing on bar dynamics the meander curvature can be considered as a fixed forcing factor.

The meaning of "instability" within bifurcation dynamics

The outcomes of this work also suggest revisiting the use of the key wording "instability", which has been often used in previous studies of river bifurcation morphodynamics, though in many times with different meanings. "Instability" has been indeed used to indicate: (i) the situation whereby an equilibrium bifurcation configuration is unstable; (ii) a systematic change of the discharge distribution over time (e.g., *Kleinhans et al.*, 2013); (iii) a bifurcation that evolves towards an highly unbalanced configuration and eventually produces the complete closure of one of the two bifurcates (e.g., *Burge*, 2006; *Le et al.*, 2018b). In this paper we have used "instability" in its mathematical meaning (i), thus indicating the mathematical instability of an equilibrium configuration (mathematical solution), which in itself could be either symmetrical or asymmetrical, and therefore may become inconsistent with meanings (ii) or (iii). Moreover, though meanings (ii) and (iii) might be interchangeable under some circumstances, this does not apply in general, and they may not be of help in disentangling the role of the free and of the forced bifurcation mechanisms when analysing a specific situation. For example, the instability of the balanced solution in the super-resonant regime does not necessarily lead to the closure of one bifurcate, but often leads to a stable, unbalanced configuration. Similarly, a partial or complete channel closure may be caused by a forcing factor rather than an instability of an equilibrium configuration, which in itself could be symmetrical or asymmetrical. This is, for instance, the case when a localized obstacle deviates the flux towards one preferred bifurcate (*Le et al.*, 2018b).

Applicability and limitations of the present approach

In this paper we have adopted a local viewpoint of the bifurcation morphodynamics, which focuses on a tile of a complex mosaic of processes where several autogenic mechanisms interact at different spatial and temporal scales (e.g., in the case of bifurcations coupled with aggrading downstream channels or embedded in braided networks).

The methodological approach can be broadly applied to analyse river bifurcations in real settings. The key ingredient required by the two-cell model to account for the upstream forcings is the availability of suitable transverse distributions of flow and sediment transport to compute water and sediment fluxes that enter the bifurcation node. Our results refer to the simple case of a relatively long channel of constant curvature, and are based on the assumption of fully developed flow, which is not satisfied in short bends and in general when the curvature is spatially varying, as in meandering channels. Extending the model to treat such complex configurations would require coupling the two-cell nodal point conditions with a sound model for flow and bed topography in meandering channels (e.g., *Zolezzi and Seminara*, 2001). This analysis is beyond the scope of the present paper; however, we may expect that in this case bifurcation stability will depend not only on local curvature, but also on the position of the bifurcation node with respect to the steady pattern of point bars forming in the upstream channel (*Le et al.*, 2018a).

Further investigation is needed to understand to what extent the key mechanisms driving the bifurcation instability, and in particular the upstream morphodynamic influence, can be affected by processes that are often not reproduced by mathematical and physical models. Specifically, two fundamental processes would probably need more consideration in future research. The first is sediment sorting: despite some indications of a relatively weak effect of grain sorting on the stability of migrating bars (*Lanzoni and Tubino*, 1999), its role in determining the bifurcation stability is not clear, especially in gravel bed channels (*Burge*, 2006). The second process is suspended sediment transport, which is often dominant in large, multi-thread, sand bed rivers (*Szupiany et al.*, 2012): when suspended load is the dominant mode of sediment transport the gravitational pull towards the deeper channel is probably weaker, so that the bifurcation may be even more unstable than currently predicted (*Kleinhans et al.*, 2006).

5 Conclusions

The present work offers a viewpoint of river bifurcations as dynamical systems for which a distinct role of the free and forced responses can be identified. We propose a theoretical framework based on the 1D model with two-cell bifurcation node originally developed by *Bolla Pittaluga et al.* (2003), as extended by *Kleinhans et al.* (2008) to account for the curvature-driven secondary flow. Furthermore, we incorporate the key outcomes of the fully 2D analytical approach of *Redolfi et al.* (2016) within the classical 1D scheme for river bifurcations. Two main forcing factors are considered, the curvature of the upstream channel and a slope advantage of one of the bifurcates, though the approach could be easily extended to account for other factors (e.g., the presence of a local obstacle upstream the bifurcation).

The key advantage of the proposed approach is its ability to clearly isolate the different free and forced mechanisms that may control the bifurcation dynamics in a complex setting, like that of real-world bifurcations, thus resulting in a suitable tool to gain clear insight in the analysis and interpretation of numerical model outcomes and of field observations. The key novel outcomes for bifurcation dynamics can be summarized in the following four items.

1. The bifurcation stability criterion based on the resonant aspect ratio threshold has been successfully tested against data of both gravel bed and sand bed channels, and it allows for capturing the opposite effects of Shields stress, which tend to promote more balanced bifurcations in gravel bed rivers and more unbalanced bifurcations in sand bed streams. This criterion can then be used for predicting the balanced/unbalanced character of free bifurcations, and it allows incorporating the fully-2D solution of *Redolfi et al.* (2016) within the classical 1D theory (*Wang et al.*, 1995; *Bolla Pittaluga et al.*, 2003) with no need to calibrate specific bifurcation parameters.

2. The role of the free instability mechanism is not limited to purely free bifurcations, but is also fundamental in the dynamics of the forced bifurcations that are more representative of real-world settings. Therefore, river bifurcations with super-resonant upstream channels are dominated by the free mechanism, characterized by multiple, highly unbalanced equilibrium configurations. This remarkable behaviour might lead to counter-intuitive outcomes, where for example water and sediment fluxes are mainly delivered towards the bifurcate located at the inner bank of a channel bend.

3. Analysis of the interaction between two of the most common forcing effects (slope advantage and curvature) allows us to quantify the parameters range where free and forcing effects cooperate or compete in determining the overall bifurcation dynamics. Under sub-resonant conditions, the interaction between upstream curvature and slope advantage is smoothly dependent on the relative intensity of the forcings (*Kleinhans et al.*, 2008; *van Dijk et al.*,

2014), while this is not the case under super-resonant conditions, for which abrupt transitions between opposite, highly unbalanced equilibrium states are expected.

4. The above results highlight how river bifurcations behave as dynamical systems like many other eco-morphological processes in rivers and freshwater bodies (e.g. *Scheffer et al.*, 2001), where the nonlinear interaction among internal and external mechanisms gives rise to a complex response, characterized by sensitivity to the initial conditions, multistable states and hysteresis cycles.

Acknowledgements

Marco Redolfi's work is supported by "Agenzia Provinciale per le Risorse Idriche e l'Energia (APRIE) - Provincia Autonoma di Trento". All data are from published works. Matlab codes for the model solution and for the computation of the resonant aspect ratio are available at `https://bitbucket.org/Marco_Redolfi/freeforced_bifurcations` and at `https://bitbucket.org/Marco_Redolfi/bars_res-crit`, respectively. This manuscript has highly benefited from the comments of Chris Paola and Gerard Salter.

Appendix A: Fully developed flow in a constant curvature channel

Here we provide a detailed derivation of the flow field in a channel of constant curvature, obtained by following the *Struiksma et al.* (1985) approach.

The model is formulated in a curvilinear system of reference $\{x, y\}$, where x is pointing in the downstream direction and y represents the transverse coordinate (see Figure 3). Assuming a fully developed flow, all dependent variables vary only with y, and therefore the x-derivatives vanish; in such conditions, the continuity equation gives zero transverse fluxes of water and sediment, while the longitudinal momentum equation reduces to an uniform flow relation for the depth-averaged longitudinal velocity U, namely:

$$U = c\sqrt{g\,S\,D}, \tag{A1}$$

where the longitudinal slope S depends on y as:

$$S = S_0 \frac{R}{R + y}, \tag{A2}$$

with S_0 indicating the slope of the channel centreline (i.e. at $y = 0$).

The longitudinal velocity generates a shear stress τ_x, which can be computed as:

$$\tau_x = \rho \frac{U^2}{c^2}, \tag{A3}$$

while the secondary flow produces a shear stress in the transverse direction, given by (see *Struiksma et al.*, 1985):

$$\tau_y = -\rho\, A \frac{DU^2}{c^2} \frac{1}{R}, \tag{A4}$$

where ρ indicates the water density.

The transverse stress τ_y needs to be compensated by a gradient of the bed elevation. Therefore, considering the *Ikeda* (1982) formulation for the effect of gravity on the sediment transport direction, the following relation arises:

$$\frac{r}{\sqrt{\theta}} \frac{d\eta}{dy} = \frac{\tau_y}{\tau_x} = -A \frac{D}{R}. \tag{A5}$$

Transverse profiles of bed elevation can be obtained by integrating Equation (A5). To this aim, we need to specify how the water depth varies along the cross section through the following geometrical relation:

$$\frac{dD}{dy} = \frac{dH}{dy} - \frac{d\eta}{dy}, \tag{A6}$$

where H indicates the water surface elevation.

Under the hypothesis of horizontal free surface, Equation (A6) reduces to $dD/dy = -d\eta/dy$, so that the differential equation (A5) can be easily solved in terms of D. More generally, the gradient of free surface elevation can be derived from the equation of transverse momentum:

$$g \frac{dH}{dy} + \frac{\tau_y}{\rho D} = \frac{U^2}{R}, \tag{A7}$$

which, when combined with Equations (A5) and (A6), gives an expression of the type:

$$\frac{dD}{dy} = fct(y, D), \tag{A8}$$

which can be easily solved by numerical integration.

The effect of the channel curvature on the transverse profiles of bed and water surface elevation is illustrated in Figure 13. The spiral flow induces higher bed elevation and slightly lower water surface elevation at the inner bend. Consequently, water depth, velocity, and water and sediment fluxes are higher at the outer bend. The resulting transverse profiles are clearly nonlinear, especially when the channel is highly curved.

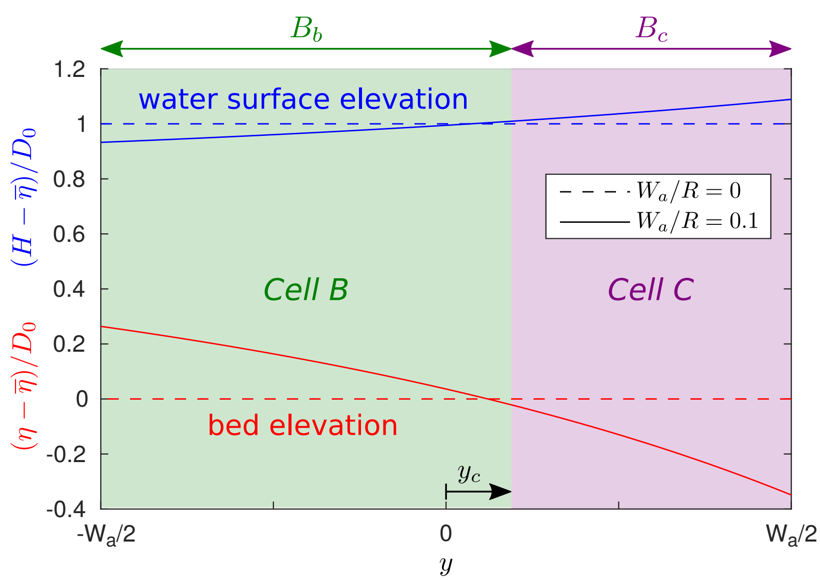

Figure 13: Transverse profiles of (scaled) bed and water surface elevation in the main channel, where $\overline{\eta}$ is the mean bed elevation. Dashed lines: straight channel; solid lines: curved channel. Parameters are $\theta_0 = 0.1$, $d_s = 0.02$, $r = 0.5$. Background colours indicate the position of the two cells of size B_b and B_c.

Once the transverse profiles are known, the input fluxes for the two-cell model can be computed by integrating along their respective domain. In the general case of different width of the downstream bifurcates (i.e. $W_b \neq W_c$), the width of the two cells (see Figure 13) can be calculated as:

$$B_b = W_a \frac{W_b}{W_b + W_c}, \qquad B_c = W_a \frac{W_c}{W_b + W_c}, \tag{A9}$$

so that the transverse position of the interface between the two cells reads:

$$y_c = B_b - \frac{W_a}{2} = \frac{W_a}{2}\left(\frac{W_b - W_c}{W_b + W_c}\right), \tag{A10}$$

which vanishes when $W_b = W_c$ as assumed in the paper. Finally, water and sediment fluxes feeding the two cells are given by the following relations:

$$Q_b^{IN} = \int_{-W_a/2}^{y_c} U D \, dy, \qquad Q_c^{IN} = 1 - Q_b^{IN}, \tag{A11}$$

$$Qs_b^{IN} = \sqrt{g\Delta d_{50}^3} \int_{-W_a/2}^{y_c} \Phi\left(\theta, \frac{D}{d_{50}}\right) dy, \qquad Qs_c^{IN} = 1 - Qs_b^{IN}. \tag{A12}$$

Appendix B: Algebraic expression for c_D, Φ_D and Φ_T coefficients

In this section we provide an explicit expression of the coefficients arising from linear stability analysis, which are needed to evaluate the critical and the resonant aspect ratio through Equations (12) and (14).

The c_D coefficient, which defines the response of the Chézy coefficient to variations of water depth, is defined as:

$$c_D := \frac{D_0}{c_0} \frac{\partial c}{\partial D}\bigg|_{D_0}. \tag{B1}$$

When considering the logarithmic formula of *Engelund and Fredsoe* (1982) (Equation (3)), we obtain:

$$c_D = \frac{2.5}{c_0}. \tag{B2}$$

where c_0 is the Chézy coefficient evaluated at reference conditions, namely:

$$c_0 = 6 + 2.5 \log\left(\frac{1}{2.5\, d_s}\right). \tag{B3}$$

Similarly, the coefficients Φ_D and Φ_T, which specify the sensitivity of the sediment transport to variations of water depth and Shields stress, are defined as:

$$\Phi_D := \frac{D_0}{\Phi_0}\frac{\partial \Phi}{\partial D}\bigg|_{\theta_0, D_0}, \qquad \Phi_T := \frac{\theta_0}{\Phi_0}\frac{\partial \Phi}{\partial \theta}\bigg|_{\theta_0, D_0}, \tag{B4}$$

and their explicit expression depends on the sediment transport formula used.

The *Engelund and Hansen* (1967) transport formula reads:

$$\Phi = 0.05\, c^2 \theta^{2.5}, \tag{B5}$$

and gives the following coefficients:

$$\Phi_D = 2\, c_D, \quad \Phi_T = 2.5. \tag{B6}$$

Transport formulae designed for bed load are often expressed in terms of θ only, and therefore Φ_D vanishes as the bed load function does not depend explicitly on water depth. For example when using the *Meyer-Peter and Muller* (1948) relation

$$\Phi = 8\,(\theta - \theta_{cr})^{1.5} \tag{B7}$$

the coefficients reads:

$$\Phi_D = 0, \quad \Phi_T = 1.5\,\frac{\theta_0}{\theta_0 - \theta_{cr}}. \tag{B8}$$

The *Parker* (1990) formula can be expressed as:

$$\Phi = 0.00218\,\theta^{1.5}\, G(\xi), \quad \xi := \frac{\theta}{0.0386}, \tag{B9}$$

where $G(\xi)$ is a piecewise-defined function:

$$G(\xi) = \begin{cases} 5474\,(1 - 0.853/\xi)^{4.5} & \xi > 1.59 \\ \exp\left[14.2(\xi - 1) - 9.28(\xi - 1)^2\right] & 1 \leq \xi \leq 1.59 \\ \xi^{14.2} & \xi < 1 \end{cases} . \tag{B10}$$

In this case we obtain:

$$\Phi_D = 0, \quad \Phi_T = 1.5 + \frac{G_\xi}{0.0386}, \quad G_\xi := \frac{\xi_0}{G_0}\frac{dG}{d\xi}, \tag{B11}$$

where G_ξ can be expressed by deriving Equation (B10), which gives:

$$G_\xi = \begin{cases} \dfrac{4.5}{\xi_0/0.853 - 1} & \xi_0 > 1.59 \\ -18.56\,\xi_0^2 + 32.76\,\xi_0 & 1 \leq \xi_0 \leq 1.59 \\ 14.2 & \xi_0 < 1 \end{cases} . \tag{B12}$$

References

Baar, A. W., J. de Smit, W. S. J. Uijttewaal, and M. G. Kleinhans (2018), Sediment Transport of Fine Sand to Fine Gravel on Transverse Bed Slopes in Rotating Annular Flume Experiments, *Water Resources Research*, *54*(1), 19–45, doi:10.1002/2017WR020604.

Bertoldi, W. (2012), Life of a bifurcation in a gravel-bed braided river, *Earth Surface Processes and Landforms*, *37*(12), 1327–1336, doi:10.1002/esp.3279.

Bertoldi, W., and M. Tubino (2007), River bifurcations: Experimental observations on equilibrium configurations, *Water Resources Research*, *43*(10), 1–10, doi:10.1029/2007WR005907.

Bertoldi, W., L. Zanoni, S. Miori, R. Repetto, and M. Tubino (2009), Interaction between migrating bars and bifurcations in gravel bed rivers, *Water Resources Research*, *45*(6), 1–12, doi:10.1029/2008WR007086.

Blondeaux, P., and G. Seminara (1985), A Unified Bar Bend Theory of River Meanders, *Journal of Fluid Mechanics*, *157*, 449–470.

Bolla Pittaluga, M., R. Repetto, and M. Tubino (2003), Correction to "Channel bifurcation in braided rivers: Equilibrium configurations and stability", *Water Resources Research*, *39*(3), 1–13, doi:10.1029/2003WR002754.

Bolla Pittaluga, M., G. Coco, and M. G. Kleinhans (2015), A unified framework for stability of channel bifurcations in gravel and sand fluvial systems, *Geophysical Research Letters*, *42*(18), 7521–7536, doi:10.1002/2015GL065175.

Burge, L. M. (2006), Stability, morphology and surface grain size patterns of channel bifurcation in gravel-cobble bedded anabranching rivers, *Earth Surface Processes and Landforms*, *31*(10), 1211–1226, doi:10.1002/esp.1325.

Camporeale, C., P. Perona, A. Porporato, and L. Ridolfi (2007), Hierarchy of models for meandering rivers and related morphodynamic processes, *Reviews of Geophysics*, *45*(1), 1–28, doi:10.1029/2005RG000185.

Edmonds, D. A. (2012), Stability of backwater-influenced river bifurcations: A study of the Mississippi-Atchafalaya system, *Geophysical Research Letters*, *39*(8), 1–5, doi:10.1029/2012GL051125.

Edmonds, D. A., and R. L. Slingerland (2008), Stability of delta distributary networks and their bifurcations, *Water Resources Research*, *44*(9), 1–13, doi:10.1029/2008WR006992.

Engelund, F., and J. Fredsoe (1982), Sediment Ripples and Dunes, *Annual Review of Fluid Mechanics*, *14*, 13–37, doi:10.1146/annurev.fl.14.010182.000305.

Engelund, F., and E. Hansen (1967), *A monograph on sediment transport in alluvial streams*, 65 pp., Tekniks Forlag, Copenhagen, Denmark, doi:10.1007/s13398-014-0173-7.2.

Federici, B., and C. Paola (2003), Dynamics of channel bifurcations in noncohesive sediments, *Water Resources Research*, *39*(6), 1162, doi:10.1029/2002WR001434.

Golubitsky, M., and D. Schaeffer (1979), An analysis of imperfect bifurcation, *Annals of the New York Academy of Sciences*, *316*(1), 127–133, doi:10.1111/j.1749-6632.1979.tb29464.x.

Grenfell, M., R. Aalto, and A. Nicholas (2012), Chute channel dynamics in large, sand-bed meandering rivers, *Earth Surface Processes and Landforms*, *37*(3), 315–331, doi:10.1002/esp.2257.

Habersack, H., and H. Piégay (2007), 27 River restoration in the Alps and their surroundings: past experience and future challenges, *Developments in Earth Surface Processes*, *11*, 703–735.

Hardy, R. J., S. N. Lane, and D. Yu (2011), Flow structures at an idealized bifurcation: A numerical experiment, *Earth Surface Processes and Landforms*, *36*(15), 2083–2096, doi:10.1002/esp.2235.

Ikeda, S. (1982), Incipient motion of sand particles on side slopes, *Journal of Hydraulic Division*, *108*(1), 95–114.

Kleinhans, M. G., B. Jagers, E. Mosselman, and K. Sloff (2006), Effect of upstream meanders on bifurcation stability and sediment division in 1D, 2D and 3D models, in *River flow 2006 : pro-*

ceedings of the International Conference on Fluvial Hydraulics, Lisbon, Portugal, 6-8 September 2006, pp. 1355–1362.

Kleinhans, M. G., H. R. A. Jagers, E. Mosselman, and C. J. Sloff (2008), Bifurcation dynamics and avulsion duration in meandering rivers by one-dimensional and three-dimensional models, *Water Resources Research*, *44*(8), 1–31, doi:10.1029/2007WR005912.

Kleinhans, M. G., K. M. Cohen, J. Hoekstra, and J. M. Ijmker (2011), Evolution of a bifurcation in a meandering river with adjustable channel widths, Rhine delta apex, The Netherlands, *Earth Surface Processes and Landforms*, *36*(15), 2011–2027, doi:10.1002/esp.2222.

Kleinhans, M. G., T. de Haas, E. Lavooi, and B. Makaske (2012), Evaluating competing hypotheses for the origin and dynamics of river anastomosis, *Earth Surface Processes and Landforms*, *37*(12), 1337–1351, doi:10.1002/esp.3282.

Kleinhans, M. G., R. I. Ferguson, S. N. Lane, and R. J. Hardy (2013), Splitting rivers at their seams: Bifurcations and avulsion, *Earth Surface Processes and Landforms*, *38*(1), 47–61, doi:10.1002/esp.3268.

Lanzoni, S., and M. Tubino (1999), Grain sorting and bar instability, *Journal of Fluid Mechanics*, *393*, 149–174, doi:10.1017/S0022112099005583.

Le, T., A. Crosato, E. Mosselman, and W. Uijttewaal (2018a), On the stability of river bifurcations created by longitudinal training walls. Numerical investigation, *Advances in Water Resources*, *113*, 112–125, doi:10.1016/j.advwatres.2018.01.012.

Le, T. B., A. Crosato, and W. S. Uijttewaal (2018b), Long-term morphological developments of river channels separated by a longitudinal training wall, *Advances in Water Resources*, *113*, 73–85, doi:10.1016/j.advwatres.2018.01.007.

Lesser, G. R., J. A. Roelvink, J. A. van Kester, and G. S. Stelling (2004), Development and validation of a three-dimensional morphological model, *Coastal Engineering*, *51*(8-9), 883–915, doi:10.1016/j.coastaleng.2004.07.014.

Meyer-Peter, E., and R. Muller (1948), Formulas for bed load transport, *Proceedings of the 2nd congress of the International Association for Hydraulic Research*, *2*, 39–64.

Miori, S., R. Repetto, and M. Tubino (2006), A one-dimensional model of bifurcations in gravel bed channels with erodible banks, *Water Resources Research*, *42*(11), 1–12, doi:10.1029/2006WR004863.

Parker, G. (1990), Surface-based bedload transport relation for gravel rivers, *Journal of Hydraulic Research*, *28*(4), 417–436, doi:10.1080/00221689009499058.

Redolfi, M., G. Zolezzi, and M. Tubino (2016), Free instability of channel bifurcations and morphodynamic influence, *Journal of Fluid Mechanics*, *799*, 476–504, doi:10.1017/jfm.2016.389.

Salter, G., C. Paola, and V. R. Voller (2018), Control of Delta Avulsion by Downstream Sediment Sinks, *Journal of Geophysical Research: Earth Surface*, pp. 1060–1067, doi:10.1002/2017JF004350.

Scheffer, M., S. Carpenter, J. A. Foley, C. Folke, and B. Walker (2001), Catastrophic shifts in ecosystems, *Nature*, *413*(6856), 591–596, doi:10.1038/35098000.

Seminara, G., and M. Tubino (1989), Alternate Bars and Meandering : Free , Forced and Mixed Interactions, in *River Meandering*, vol. 12, edited by S. Ikeda and G. Parker, pp. 267 – 320, AGU, Washington, D.C.

Siviglia, A., G. Stecca, D. Vanzo, G. Zolezzi, E. F. Toro, and M. Tubino (2013), Numerical modelling of two-dimensional morphodynamics with applications to river bars and bifurcations, *Advances in Water Resources*, *52*, 243–260, doi:10.1016/j.advwatres.2012.11.010.

Slingerland, R., and N. D. Smith (2004), River Avulsions and Their Deposits, *Annu. Rev. Earth Planet. Sci.*, *32*(1), 257–285, doi:10.1146/annurev.earth.32.101802.120201.

Sloff, K., and E. Mosselman (2012), Bifurcation modelling in a meandering gravel-sand bed river, *Earth Surface Processes and Landforms*, *37*(14), 1556–1566, doi:10.1002/esp.3305.

Struiksma, N., K. W. Olesen, C. Flokstra, and H. J. De Vriend (1985), Bed deformation in curved alluvial channels, *Journal of Hydraulic Research*, *23*(1), 57–79, doi:10.1080/00221688509499377.

Szupiany, R. N., M. L. Amsler, J. Hernandez, D. R. Parsons, J. L. Best, E. Fornari, and A. Trento (2012), Flow fields, bed shear stresses, and suspended bed sediment dynamics in bifurcations of a large river, *Water Resources Research*, *48*(11), 1–20, doi:10.1029/2011WR011677.

Tubino, M., and G. Seminara (1990), Free–forced interactions in developing meanders and suppression of free bars, *Journal of Fluid Mechanics*, *214*, 131–159, doi:10.1017/S0022112090000088.

Van der Mark, C. F., and E. Mosselman (2013), Effects of helical flow in one-dimensional modelling of sediment distribution at river bifurcations, *Earth Surface Processes and Landforms*, *38*(5), 502–511, doi:10.1002/esp.3335.

van Dijk, W. M., F. Schuurman, W. I. V. D. Lageweg, and M. G. Kleinhans (2014), Bifurcation instability and chute cutoff development in meandering gravel-bed rivers, *Geomorphology*, *213*, 277–291, doi:10.1016/j.geomorph.2014.01.018.

Wang, Z., M. De Vries, R. Fokkink, and A. Langerak (1995), Stability of river bifurcations in 1D morphodynamic models, *Journal of Hydraulic Research*, *33*(6), 739–750, doi:10.1080/00221689509498549.

Wiggins, S. (2003), *Introduction to Applied Nonlinear Dynamical Systems and Chaos*, *Texts in Applied Mathematics*, vol. 2, Springer-Verlag, New York, doi:10.1007/b97481.

Zhang, W., H. Feng, A. J. F. Hoitink, Y. Zhu, F. Gong, and J. Zheng (2017), Tidal impacts on the subtidal flow division at the main bifurcation in the Yangtze River Delta, *Estuarine, Coastal and Shelf Science*, *196*, 301–314, doi:10.1016/j.ecss.2017.07.008.

Zolezzi, G., and G. Seminara (2001), Downstream and upstream influence in river meandering. Part 1. General theory and application to overdeepening, *Journal of Fluid Mechanics*, *438*, 213–230, doi:10.1017/S002211200100427X.

Zolezzi, G., M. Guala, D. Termini, and G. Seminara (2005), Experimental observations of upstream overdeepening, *Journal of Fluid Mechanics*, *531*, 191–219, doi:10.1017/S0022112005003927.

Zolezzi, G., W. Bertoldi, and M. Tubino (2006), Morphological analysis and prediction of river bifurcations, in *Braided Rivers: Process, Deposits, Ecology and Management*, vol. 36, edited by G. H. Best, J. L. Bristow, and C. S. Petts, pp. 233–256, Blackwell, doi:10.1002/9781444304374.ch11.

Zolezzi, G., R. Luchi, and M. Tubino (2009), Morphodynamic regime of gravel bed, single-thread meandering rivers, *Journal of Geophysical Research: Earth Surface*, *114*(1), doi:10.1029/2007JF000968.